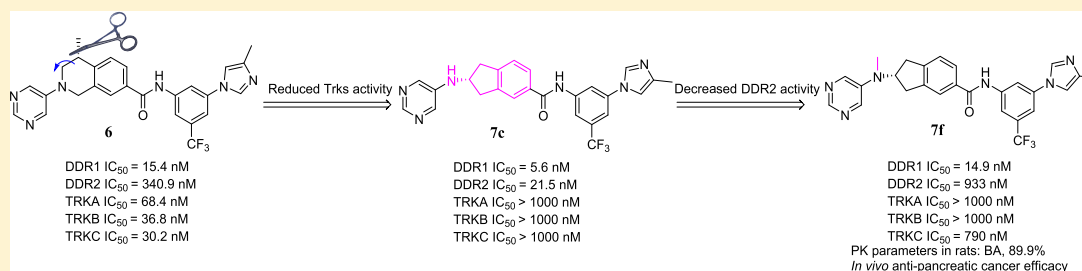


2-Amino-2,3-dihydro-1*H*-indene-5-carboxamide-Based Discoidin Domain Receptor 1 (DDR1) Inhibitors: Design, Synthesis, and in Vivo Antipancreatic Cancer EfficacyDongsheng Zhu,^{†,‡,⊥} Huocong Huang,^{§,⊥} Daniel M. Pinkas,^{||,⊥} Jinfeng Luo,[‡] Debolina Ganguly,[§] Alice E. Fox,^{||} Emily Arner,[§] Qiuping Xiang,[‡] Zheng-Chao Tu,[‡] Alex N. Bullock,^{*,||} Rolf A. Brekken,^{*,§} Ke Ding,^{*,†} and Xiaoyun Lu^{*,†}[†]International Cooperative Laboratory of Traditional Chinese Medicine Modernization and Innovative Drug Development of Chinese Ministry of Education (MOE), School of Pharmacy, Jinan University, 601 Huangpu Avenue West, Guangzhou 510632, China[‡]Guangzhou Institutes of Biomedicine and Health, Chinese Academy of Sciences, 190 Kaiyuan Avenue, Guangzhou 510530, China[§]Division of Surgical Oncology, Department of Surgery and Hamon Center for Therapeutic Oncology Research, UT Southwestern, Dallas, Texas 75390-8593, United States^{||}Structural Genomics Consortium, University of Oxford, Old Road Campus Research Building, Roosevelt Drive, Oxford OX3 7DQ, U.K.

Supporting Information



ABSTRACT: A series of 2-amino-2,3-dihydro-1*H*-indene-5-carboxamides were designed and synthesized as new selective discoidin domain receptor 1 (DDR1) inhibitors. One of the representative compounds, 7f, bound with DDR1 with a K_d value of 5.9 nM and suppressed the kinase activity with a half-maximal (50%) inhibitory concentration value of 14.9 nM. 7f potently inhibited collagen-induced DDR1 signaling and epithelial–mesenchymal transition, dose-dependently suppressed colony formation of pancreatic cancer cells, and exhibited promising in vivo therapeutic efficacy in orthotopic mouse models of pancreatic cancer.

INTRODUCTION

Pancreatic cancer, also known as the “king of cancer” with a 5 year survival rate less than 7%, is lacking effective therapies.¹ Intrinsic and/or acquired chemoresistance to the first-line drug gemcitabine is a major reason for the poor prognosis. Collective studies suggested that desmoplasia and tumor microenvironment (TME) are the key contributors to chemoresistance of pancreatic cancer patients. Desmoplasia (or desmoplastic reaction) is a prominent pathological characteristic of pancreatic cancer, resulting from the rapid expansion of cancer-associated fibroblasts and increased deposition of extracellular matrix (ECM) components. Numerous studies have shown that ECM is heavily involved in pancreatic cancer development, immune evasion, and therapy resistance. Therefore, stroma-targeting therapy becomes an attractive strategy to improve therapeutic response.² Collagens are the most abundant components in ECM.³ Biological functions of collagens are mainly mediated by two

types of receptors, integrins and discoidin domain receptors (DDRs).^{4,5} DDrs belong to the receptor tyrosine kinase (RTK) family. Two members of DDrs (DDR1 and DDR2) have been identified to date.⁶ DDR1 is predominantly expressed in epithelial cells, whereas DDR2 is typically found in cells of connective tissues. Dysregulation of DDR1 is frequently detected in a variety of human cancers and involved in several key cellular processes, such as cell differentiation, proliferation, adhesion, migration, and invasion.^{7,8} Studies have shown that DDR1 overexpression mediates pro-survival signals and metastasis in breast cancer and gastric cancer and is also involved in the recurrence of certain types of cancers.^{9–11} DDR1 has also been demonstrated to contribute to epithelial–mesenchymal transition (EMT) in pancreatic cancer.^{12,13} Pharmacological inhibition of DDR1 by a selective DDR1

Received: February 27, 2019

Published: July 16, 2019

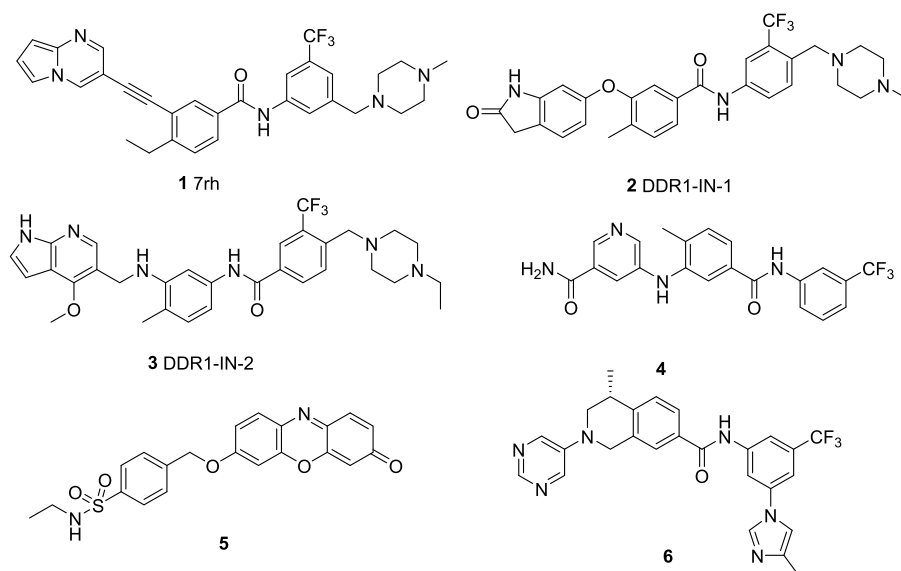


Figure 1. Reported selective DDR1 inhibitors.

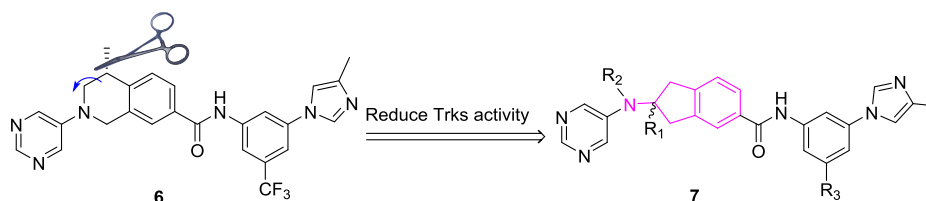


Figure 2. Design of 2-amino-2,3-dihydro-1H-indene-5-carboxamide derivatives 7 as new Trks-sparing selective DDR1 inhibitors.

inhibitor **7rh** (compound **1**, Figure 1) successfully slowed tumor progression and enhanced chemosensitivity to standard-of-care pancreatic cancer regimens.¹⁴ Therefore, DDR1 is being considered as a novel molecular target for drug discovery against pancreatic cancer.

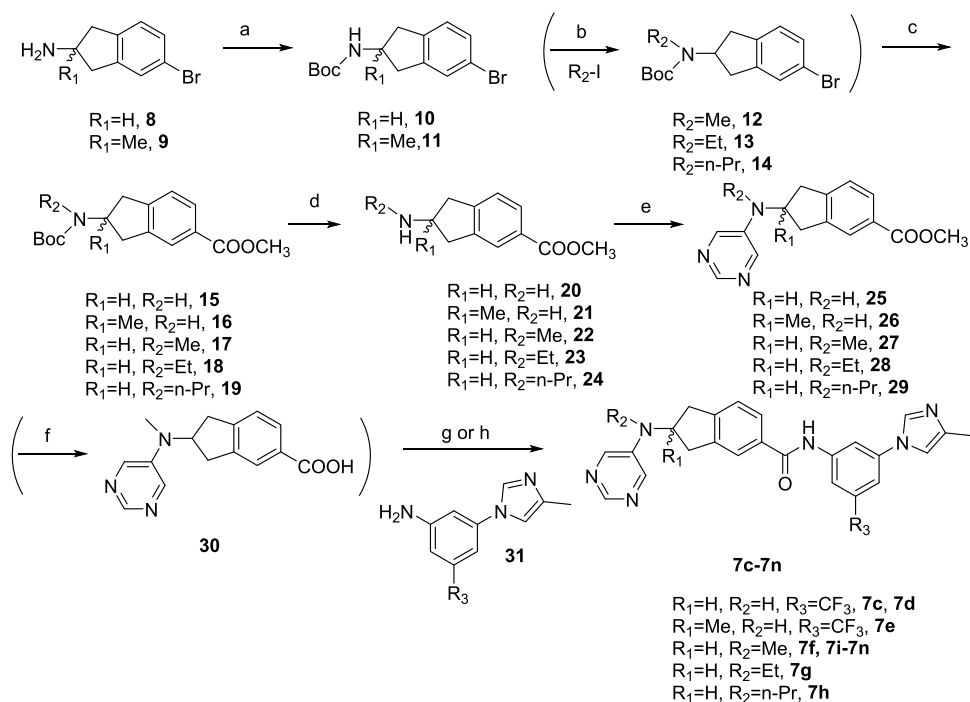
A number of DDR inhibitors have been reported (Figure 1),^{15–21} among which compound **1** (**7rh**)¹⁶ represents one of the first disclosed selective DDR1 inhibitors. This compound demonstrated promising therapeutic potential in a variety of human cancer models including pancreatic cancer,¹⁴ nonsmall cell lung cancer,²² and gastric carcinoma.¹⁰ Most recently, tetrahydroisoquinoline-7-carboxamide derivatives were also designed and synthesized as highly selective DDR1 inhibitors exhibiting *in vivo* efficacy in mouse models of inflammation-mediated pulmonary fibrosis and acute lung injury.^{21,23} Compound **6** represents one of the most selective DDR1 inhibitors to date, which exhibited an half-maximal (50%) inhibitory concentration (IC_{50}) value of 15.4 nM against DDR1 kinase, whereas it is significantly less potent for the majority of a panel of 403 other kinases. The major “off-targets” include tropomyosin receptor kinases B and C (TrkB and TrkC, respectively) with corresponding binding affinities (K_d values) of 22 and 18 nM, respectively. Further kinase assay determination confirmed that this molecule inhibited TrkA, B, and C, with IC_{50} values of 68.4, 36.8, and 30.2 nM, respectively. Trks are a family of receptor tyrosine kinases (RTKs), which are activated by neurotrophin hormones and regulate synaptic plasticity and strength in the mammalian nervous system.²⁴ Lack of Trks significantly affects the development of central and peripheral nervous systems.^{25,26} For instance, the population of corneal sensory neurons is

markedly depleted in TrkA (–/–) mice, animals lacking TrkB in parvalbumin-positive cells displayed sexually dimorphic behavioral phenotypes, whereas TrkC knockout mice exhibited profound deficiencies in CNS glial cells.²⁷ Thus, “off-targeting” Trks may raise some concerns about the potential neurotoxicity issues of the previously reported DDR1 inhibitors. With the aim to improve the target specificity, a series of 2-amino-2,3-dihydro-1H-indene-5-carboxamide derivatives were designed and synthesized as new Trks-sparing DDR1 inhibitors. Moreover, the potential therapeutic effects on pancreatic cancer were also investigated by utilizing *in vitro* and *in vivo* models (Figure 2).

Syntheses of the designed compounds **7a**, **7b**, and **7c–n** are described in Schemes S1 and 1, respectively. Briefly, protection of **8** and **9** with $(Boc)_2O$ gave **10** and **11**, respectively. Further alkylation of **10** generated **12–14**. **10–14** were converted to **15–19** by using a carbonyl-extrusion reaction, which were deprotected by hydrochloric acid to produce intermediates **20–24**. Coupling of **20–24** with 5-bromopyrimidine through a Buchwald–Hartwig amination reaction provided **25–29**. The ester **27** was hydrolyzed to **30**. **25–30** were further reacted with **31** to produce the final compounds **7c–n**.

RESULTS AND DISCUSSION

Compound **6** is a selective DDR1 inhibitor designed and synthesized in our laboratory. However, this compound displayed similar off-target potency against TrkA, TrkB, and TrkC with IC_{50} values of 68.4, 36.8, and 30.2 nM, respectively (Table 1). Off-target inhibition against Trks may raise some concern about the potential neurotoxicity issues of the molecule. Aiming to improve the target specificity, we first

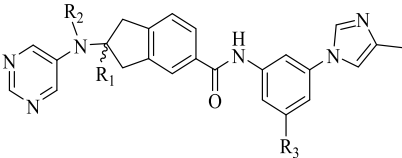
Scheme 1. Syntheses of Compounds 7c–n^a

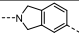
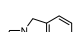


^aReagents and conditions: (a) di-*tert*-butyl dicarbonate (Boc_2O), triethylamine (Et_3N), 90–95%; (b) sodium hydride (NaH), *N,N*-dimethylformamide (DMF), iodomethane, **12**; iodoethane, **13**; 1-iodopropane, **14**; 50–80%; (c) palladium(II) acetate ($Pd(OAc)_2$), Et_3N , carbon monoxide (CO), 100 °C, 50–70%; (d) 4 M HCl, 50 °C; (e) bis(dibenzylideneacetone)palladium ($Pd(dba)_2$), 2-dicyclohexylphosphino-2',6'-diisopropoxybiphenyl (Ruphos), cesium carbonate (Cs_2CO_3), 5-bromopyrimidine, 80 °C, 30–40%; (f) 1 M sodium hydroxide ($NaOH$), dioxane, 98%; (g) potassium *tert*-butoxide (*t*-BuOK), –20 °C to room temperature (rt), 30–70%; (h) 2-(7-aza-1*H*-benzotriazole-1-yl)-1,1,3,3-tetramethyluronium hexafluorophosphate, *N,N*-diisopropylethylamine (DIPEA), 20–55%.

docked compound **6** into the adenosine triphosphate (ATP)-binding site of TrkC [Protein Data Bank (PDB) ID: 3V5Q].²⁸ It was shown that the compound could bind well to TrkC with a Asp-Phe-Gly (DFG)-out conformation, which was similar to the binding mode with DDR1 (Figure 3A,B).²¹ The only small difference between binding modes of **6** with DDR1 and TrkC is that the methyl group on tetrahydroisoquinoline occupied a small hydrophobic pocket formed by Val552, Ala570, Lys572, and Phe617 to achieve some hydrophobic interactions in TrkC. Thus, it was predicted that diminishing this interaction might decrease the binding with Trks and improve DDR1 target selectivity of the molecule. Based on this hypothesis, an isoindoline scaffold was first utilized to replace the 1-methyl tetrahydroisoquinoline in **6** to generate compounds **7a** and **7b**. Disappointingly, both **7a** and **7b** lost all of the DDR1 inhibitory activity, although the modification indeed abolished the off-target inhibition against Trks (Table 1). Further computational investigation demonstrated that **7a** failed to fit nicely into the DDR1 ATP binding pocket (PDB ID: 5FDP, data not shown),²¹ whereas compound **7b** could form weak hydrogen bonds (HBs) with the hinge residue Met704, but there was no other interaction between the isoindoline scaffold and DDR1 (Figure S1). The computational study also indicated that the methylene moiety of **7b** is accessible to the gatekeeper Thr701 residue, and it could be replaced by a hydrogen bond donor moiety to form a hydrogen bond interaction with Thr701 to potentially improve the DDR1 inhibitory activity. To validate this hypothesis, 2-amino-2,3-dihydro-1*H*-indene-5-carboxamide enantiomers **7c** and **7d** were designed and synthesized by moving the nitrogen atom

out of the original isoindoline ring. It was also predicted that the *R*-isomer **7c** might achieve a more favorable binding with DDR1 than that of the *S*-isomer **7d** to form a hydrogen bond with the gatekeeper residue Thr701 (Figure S2A,B). Indeed, kinase inhibition determination showed that compound **7c** potentially inhibited DDR1 with an IC_{50} value of 5.6 nM, whereas the corresponding value for **7d** was 42.5 nM. Compound **7c** exhibited a similar suppressive activity against DDR2 with an IC_{50} value of 21.5 nM. It was also noteworthy that **7c** almost totally abolished the inhibitory potencies against Trks with IC_{50} values greater than 1000 nM. However, introduction of a methyl group at the R_3 -position (**7e**) caused an approximately 129-fold potency loss, which might be due to the steric hindrance to interfere with potential hydrogen bond formation.

A 2.0 Å resolution X-ray crystallographic structure of **7c** and the DDR1 complex was determined to elucidate details of the interaction (Figure 3C and Table S2). It was shown that **7c** fitted nicely into the ATP binding pocket of DDR1 with a typical type II binding mode. The nitrogen atom of pyrimidine was observed to form a hydrogen bond with hinge residue Met704, whereas the amino group at 2-position of the indene formed a hydrogen bond with gatekeeper residue Thr701. Two additional hydrogen bonds were also observed, one between the amide nitrogen of **7c** and the carboxylates of Glu672 and another between the amide carbonyl of **7c** and the backbone amide nitrogen of Asp784. Additionally, the trifluoromethyl group was observed to fit snugly into the DFG-out pocket. A computational study was further performed to rationalize the significant potency loss for Trks (PDB ID: 3V5Q).¹⁸ It was

Table 1. In Vitro Kinase Inhibitory Activities of Compounds 7a–n against DDR1, DDR2, TrkA, TrkB, and TrkC^{a,b}


Cpds	R/S	R ₁	R ₂	R ₃	Kinase inhibition IC ₅₀ (nM)				
					DDR1 ^a	DDR2 ^a	TrkA ^b	TrkB ^b	TrkC ^b
7a	/			CF ₃	>1000	>1000	>1000	>1000	>1000
7b	/			CF ₃	>1000	>1000	>1000	>1000	>1000
7c	R	H	H	CF ₃	5.6±0.2	21.5±1.3	>1000	>1000	>1000
7d	S	H	H	CF ₃	42.5±7.0	634±53.5	365.7±1.8	343.9±44.3	46.3±28.6
7e	R/S	Me	H	CF ₃	723.1±199.0	>1000	>1000	>1000	>1000
7f	R	H	Me	CF ₃	14.9±1.4	933±29	>1000	>1000	790±205
7g	R	H	Et	CF ₃	150.5±20.0	>1000	398.3±90	569±191	278±70
7h	R	H	<i>n</i> -Pr	CF ₃	>1000	>1000	>1000	>1000	>1000
7i	R	H	Me	Me	638.9±42.0	>1000	>1000	>1000	>1000
7j	R	H	Me	Et	14.7±0.9	467±20.0	400±98.3	>1000	364.2±25.6
7k	R	H	Me	<i>i</i> -Pr	15.5±3.3	207.3±10.9	326.3±108.5	145.4±35.5	215.4±61.5
7l	R	H	Me	<i>t</i> -Bu	14.4±1.1	102.2±0.1	174.0±38	270.7±29	158.9±35
7m	R	H	Me	cyclohexyl	68.7±1.1	>1000	>1000	>1000	>1000
7n	R	H	Me	adamantyl	>1000	>1000	>1000	>1000	>1000
6					15.4±1.5	340.9±27	68.4±14.6	36.8±4.4	30.2±6.5

^aDDR1 and DDR2 inhibition assays were performed using the LANCE ULTRA kinase assay. ^bTrkA/B/C activity was performed using the fluorescence resonance energy transfer (FRET)-based Z'-Lyte assay. The data are mean values from at least three independent experiments.

shown that the pyrimidinyl moiety of 7c would still be able to form a hydrogen bond (~3.1 Å) with the key residue Met620 in TrkC (Figure 3D), but the gatekeeper Phe617 of TrkC altered the three-dimensional (3D) structure of the ATP pocket relative to DDR1, which would both preclude a key hydrogen bond and additionally introduce a steric clash with 7c.

Aiming to improve DDR1 target specificity, further structural optimization was conducted. Superposition of DDR1 (PDB: 6HP9, gray) and a homology model of DDR2 (orange)²⁹ indicated that DDR1 possessed a small hydrophobic groove formed by Ile685, Thr701, and Asp703, whereas no such pocket existed in DDR2 because of its outward shifting of Glu93 and Ile76 (Figure 4A). Based on this observation, it was hypothesized that a small hydrophobic substituent might be introduced at the nitrogen atom of 7c to improve the DDR1 selectivity. Thus, compounds 7f–h, in which a methyl, ethyl, or *n*-propyl group was introduced at the corresponding position, respectively, were designed and synthesized. It was shown that the methylated compound 7i indeed significantly decreased the DDR2 inhibitory potency with an IC₅₀ of 933 nM, although it also caused a 2.6-fold potency loss for DDR1 with an IC₅₀ value of 14.9 nM (Table 1). However, both 7g and 7h resulted in 26.8- and approximately 200-fold DDR1 potency decreases, respectively.

Computational investigation supported the idea that a methyl group (7f) could fit into a small hydrophobic pocket formed by Ile685, Thr701, and Asp702, whereas loss of a hydrogen bond with Thr701 would contribute to the DDR1 potency decrease (Figure 4B).

Further structure–activity relationship investigation also revealed that the trifluoromethyl of 7f could be replaced by the ethyl (7j), isopropyl (7k), or tertiary butyl (7l) group without obviously affecting the DDR1 inhibitory potency. For instance, compounds 7j–l exhibited IC₅₀ values of 14.7, 15.0, and 14.4 nM, respectively. However, their potencies against DDR2 and Trks were improved, which made the compound less selective. A replacement of the trifluoromethyl with a methyl group (7i) caused an approximately 43-fold decrease in DDR1 potency. When the trifluoromethyl was replaced with a cyclohexyl group, the resulting compound 7m was also 5-fold less potent than the lead molecule 7f. Significantly, the amantadine derivative (7n) totally abolished its activity against DDR1 with an IC₅₀ value greater than 2.0 μM. Collectively, 7f represents one of the most potent and selective DDR1 inhibitors in the series for further biological investigation.

The binding affinity determination showed that 7f tightly bound to the ATP-binding sites of DDR1 with a K_d value of 5.9 nM (DiscoverX, San Diego, CA).³⁰ Further target specificity of 7f was investigated by KINOMEScan profiling

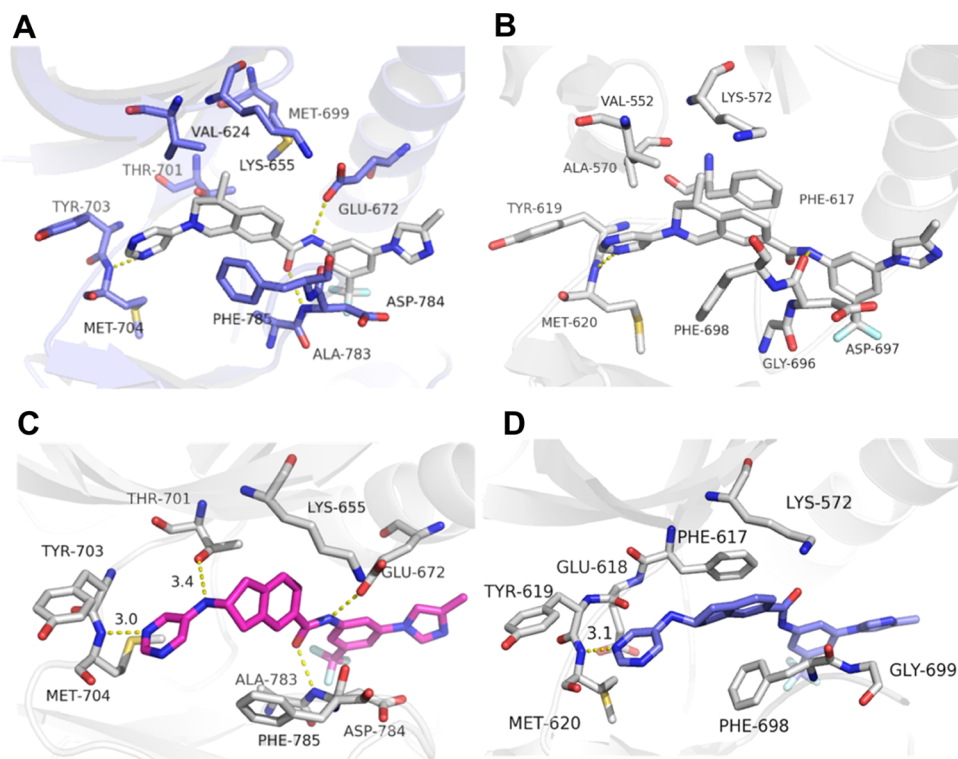


Figure 3. (A) Molecular docking of **6** into DDR1 (PDB: 5FDP). (B) Molecular docking of **6** into TrkC (PDB: 3V5Q). (C) Cocystal structures of DDR1 and **7c** (PDB: 6HP9). (D) Molecular docking of **7c** into TrkC. Compounds **6** and **7c** are shown in gray, purple, and blue stick structure. The key residues of DDR1 and TrkC kinase are shown in blue and gray stick and ribbon representation. Hydrogen bonds are indicated by yellow dashed lines to key amino acids.

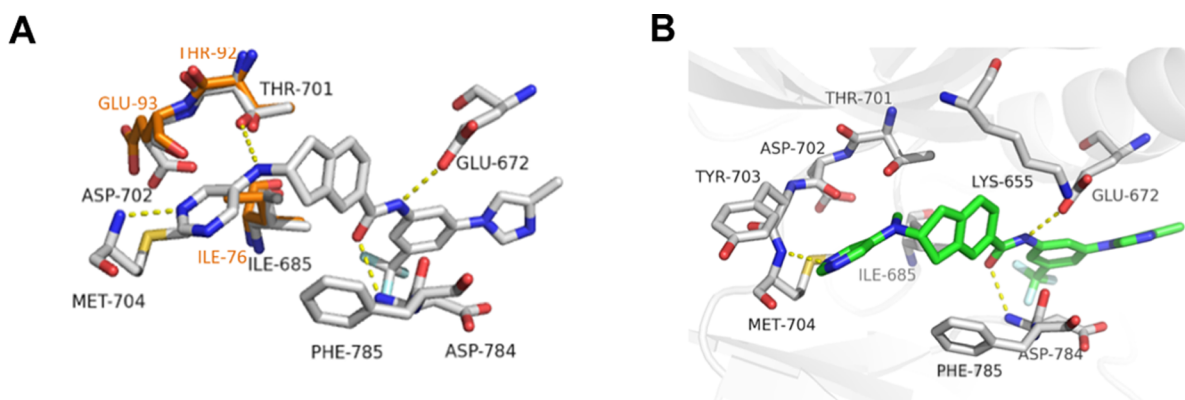


Figure 4. (A) Superposition of DDR1 (PDB: 6HP9) and DDR2. (B) Molecular docking of **7f** into DDR1 (PDB: 6HP9). The key residues of DDR1 kinase are shown in gray stick representation and DDR2 kinase are shown in orange. Compounds **7c** and **7f** are shown in gray and green stick structures, respectively. Hydrogen bonds are indicated by yellow dashed lines to key amino acids.

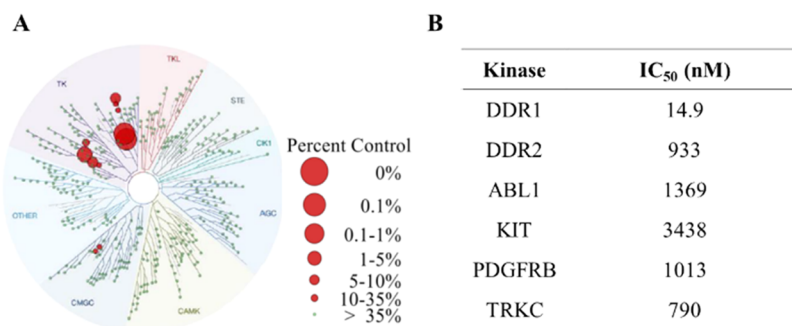


Figure 5. Target selectivity of **7f**. (A) KINOMEScan profiles for **7f**. (B) Inhibitory activities (IC₅₀) of compound **7f** against the potential off-targets.

with a panel of 468 kinases at 1.0 μM (Figure 5A). The results indicated that 7f displayed an extraordinary target selectivity with S (10) and S (1) scores of 0.015 and 0.007, respectively (Table S3). The major off-targets (inhibition > 90%, ctrl% < 10) included the DDR2, ABL1, KIT, PDGFRB, and TrkC. The inhibitory activities (IC_{50}) of 7f against above-mentioned off-targets were further determined with our in-house kinase assays (Figure 5B). It was shown that 7f displayed significantly less potencies to all of the off-target kinases.

To investigate the inhibitory effects of 7f on the biological functions of DDR1, we first examined the DDR1 signaling pathway with the drug treatment in a mouse pancreatic cancer cell line Pan02 (Figure 6). It was found that 7f dose-

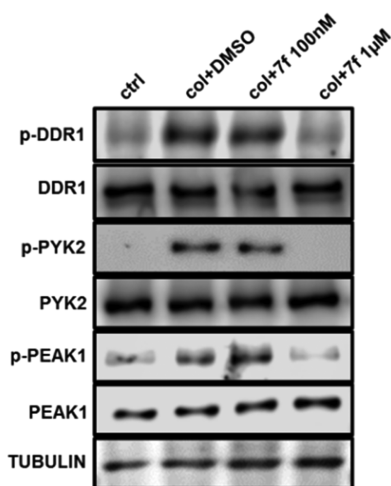


Figure 6. 7f inhibits DDR1 activation induced by collagen in vitro. Pan02 were treated with collagen I (50 $\mu\text{g}/\text{mL}$) and dimethyl sulfoxide (DMSO) or different concentrations of 7f for 8 h. Cell lysates were harvested and subjected to western blot, probing for p-DDR1, DDR1, p-PYK2, PYK2, p-PEAK1, PEAK1, and TUBULIN.

dependently inhibited collagen-induced activation of DDR1 and its downstream signaling proteins, for example, proline-rich tyrosine kinase 2 (PYK2) and pseudopodium-enriched atypical kinase 1 (PEAK1).

The activation of DDR1–PYK2–PEAK1 signaling has been shown to mediate the tumor-promoting functions of collagen, including an important process of EMT called cadherin switching,³¹ in which cancer cells specifically upregulate the mesenchymal cell adhesion protein N-cadherin, whereas the epithelial cell adhesion protein E-cadherin may or may not be affected. As a result of N-cadherin upregulation, cancer cells become substantially more motile and aggressive.³² Therefore, we performed immunofluorescence staining for E-cadherin and N-cadherin in Pan02 and another mouse pancreatic cancer cell line BMF-A3 derived from *KPfc* (*Kras*^{LSL-G12D}; *Trp53*^{lox/lox}; *Ptf1a*^{Cre/+}) mice, a genetically engineered mouse model of pancreatic cancer, to explore the effects of 7f on inhibiting DDR1-mediated cadherin switching (Figure 7A). Consistently, 7f markedly inhibited cadherin switching in each cell line regardless of the different genetic background. Moreover, we also found that 7f significantly inhibited the migratory capability of the cells in a wound-healing assay (Figure 7B).

Cell heterogeneity is a major cause of therapy resistance in most types of cancers.³³ To understand whether 7f had similar effects on inhibiting cadherin switching in different cancer cell populations derived from the same tumor, we performed a 3D

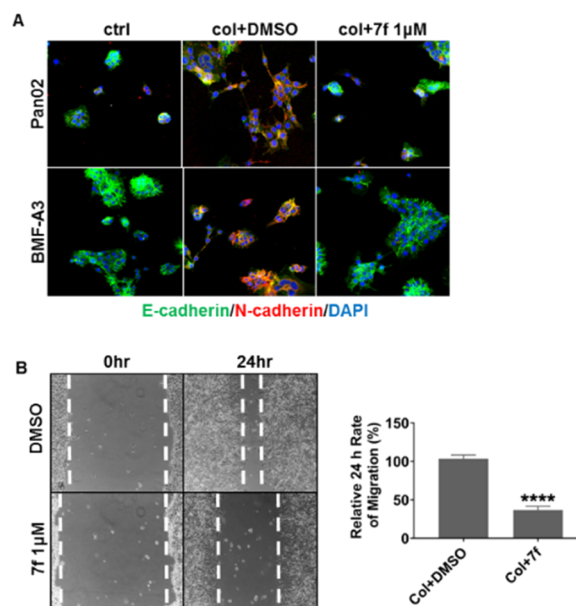


Figure 7. 7f inhibits collagen-induced cadherin switching and migration in pancreatic cancer. (A) Pan02 and primary mouse pancreatic cancer cell line BMF-A3 were treated with collagen I (50 $\mu\text{g}/\text{mL}$) and DMSO or 1 μM 7f for 24 h. Cells were fixed with methanol and stained with E-cadherin (green), N-cadherin (red), and 4',6-diamidino-2-phenylindole (DAPI, blue). Fluorescent images were captured at 20 \times magnification. (B) Wound-healing assay was performed with Pan02 cells. Cells were treated with collagen I (50 $\mu\text{g}/\text{mL}$) and DMSO or 1 μM 7f for 24 h, and relative rates of migration were measured after a 24 h period of time. **** $P < 0.0001$.

culture experiment with two different cancer cell clones derived from a *KPfc* tumor (BMF-A3 and CT1A-C11). In the presence of ECM that mimics the in vivo tumor micro-environment.³⁴ We found that BMF-A3 represented a more epithelial phenotype, which remained as clusters under 3D culture, whereas CT1A-C11 was more mesenchymal and aggressive, with an elongated and fibroblastic morphology. However, we found that 7f strongly inhibited such a mesenchymal phenotype (Figure 8A). We also examined the effect of 7f on DDR1-induced cadherin switching in the two cell lines by probing for E-cadherin and N-cadherin expressions in cell lysates. We found that although the two cell lines had different phenotypes in 3D culture, 7f inhibited the upregulation of N-cadherin similarly in a dose-dependent manner (Figure 8B). This suggests that 7f may have effects on many cancer cell populations despite cellular heterogeneity.

In addition, we examined the effects of 7f on the tumorigenicity of pancreatic cancer cells using an in vitro colony formation assay. As shown in Figure 9A,B, 7f dose-dependently inhibited colony formation significantly in BMF-A3 and Pan02 cells. However, the direct effect against proliferation of 7f seemed to be moderate, measured by cell proliferation in two-dimensional with BMF-A3 and Pan02 cells showing IC_{50} s values of 4.26 and 11.92 μM , respectively (Figure S4).

Given the effects of 7f on pancreatic cancer cells in vitro, we further studied its effects in vivo. First, we profiled the in vivo pharmacokinetics (PK) of 7f in Sprague-Dawley (SD) rats (Table 2). 7f displayed an ideal PK profile with an oral area under curve (AUC) value of 80 535 $\mu\text{g}/(\text{L h})$, a $T_{1/2}$ value of

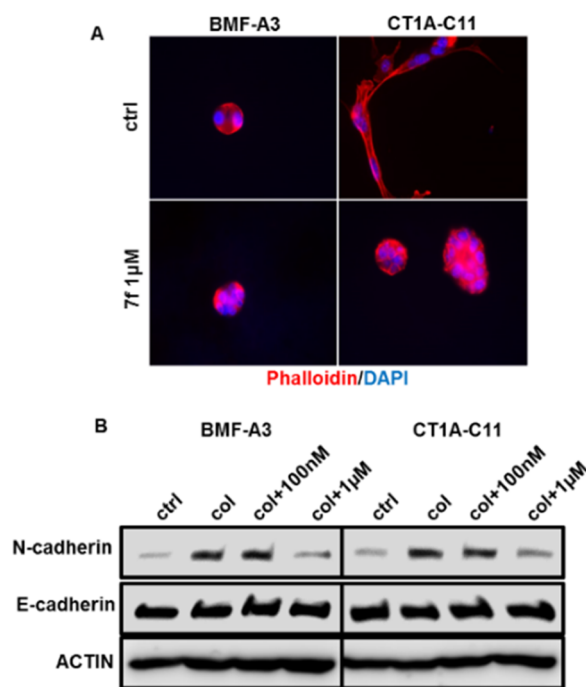


Figure 8. 7f inhibits collagen-induced cadherin switching in different cancer cell clones from *KPfc* mice. (A) BMF-A3 and CT1A-C11 were embedded in ECM consisting of 5 mg/mL matrigel and 2.1 mg/mL collagen I. Cultures were overlaid with Dulbecco's modified Eagle's medium (DMEM) + 10% fetal bovine serum (FBS) containing 2% matrigel. After 48 h, cells were fixed with methanol and stained with phalloidin (red) and DAPI (blue). Fluorescent images were captured at 20 \times magnification. (B) Primary mouse pancreatic cancer cell lines BMF-A3 and CT1A-C11 were treated with collagen I (50 μ g/mL) and DMSO or different concentrations of 7f for 18 h. Cell lysates were harvested and subjected to western blot, probing for N-cadherin, E-cadherin, and ACTIN.

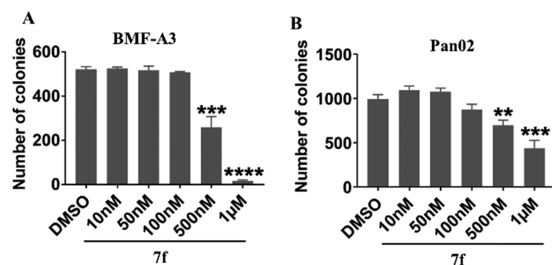


Figure 9. 7f inhibits colony formation in BMF-A3 (A) and Pan02 (B) pancreatic cancer cells. Colony formation for cells was grown in DMEM with 10% FBS \pm 7f at the indicated doses for 10 days. Mean \pm standard deviation (S.D.) colonies are shown. ** $P < 0.01$, **** $P < 0.001$, ***** $P < 0.0001$ by Student's *t*-test vs DMSO.

Table 2. Pharmacokinetic Profile of Compound 7f in Rats^a

	po (25 mg/kg)	iv (5 mg/kg)
AUC(0– ∞) μ g/(L h)	80 535.0	16 855.5
$T_{1/2}$ (h)	1.7	0.9
T_{max} (h)	4.0	0.083
C_{max} (μ g/L)	15 352.5	14 746.0
BA (%)	89.9	

^aSD rats (male, three animals per group) weighted 180–220 g were used for the study.

1.7 h, and an oral bioavailability of 89.9%, which provides the foundation for an in vivo dosing regimen.

We then established syngeneic models of pancreatic cancer by orthotopically implanting the BMF-A3 and Pan02 cells in C57BL/6 mice and evaluated the efficacy of 7f on pancreatic cancer progression. The animals were orally (po) administered vehicle or 7f [twice per day (bid), 25 and 50 mg/(kg day)] for 3 weeks. In both tumor models, 7f inhibited the progression of the tumors significantly without obviously caused animal body weight loss (Table S4), highlighting the in vivo efficacy of the molecule in pancreatic cancer (Figure 10).

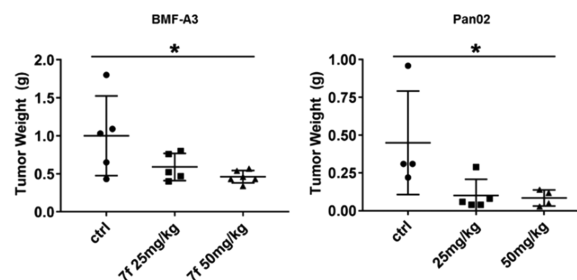


Figure 10. 7f inhibits pancreatic cancer progression in vivo. Mouse pancreatic cancer cell lines BMF-A3 and Pan02 were implanted orthotopically in C57BL/6 mice. 10 days after implantation, mice ($n = 4$ –5 per group) were orally administered with vehicle or 7f (25 and 50 mg/kg) twice per day for 3 weeks. Data were analyzed by analysis of variance (ANOVA) and presented as the mean \pm S.D. * $P < 0.05$.

CONCLUSIONS

In summary, a series of 2-amino-2,3-dihydro-1*H*-indene-5-carboxamide derivatives were designed and synthesized as novel highly selective DDR1 inhibitors with a structure-based drug design method. Compound 7f strongly suppressed DDR1 with an IC_{50} value of 14.9 nM, but it was significantly less potent against a panel of other 403 nonmutated kinases at 1.0 μ M. 7f also potently inhibited the collagen-induced cadherin switching event induced by DDR1 and dose-dependently suppressed colony formation of pancreatic cancer cells. Moreover, 7f demonstrated good pharmacokinetic properties and promising therapeutic effect by oral administration in orthotopic syngenic models of pancreatic cancer. Notably, several somatic mutations of DDR1 had been clinically identified, but most of them are located out of the kinase domain.³⁵ Thus, 7f may achieve similar inhibition against these disease-related mutants. Extensive biological investigation is undergoing to validate 7f as a lead molecule for further development.

EXPERIMENTAL SECTION

General Chemistry. Reagents and solvents were purchased from commercial sources and used directly. Flash chromatography was performed using 300-mesh silica gel. Reactions were monitored by thin-layer chromatography using silica gel plates with fluorescence F_{254} and UV light visualization. Low-resolution electrospray ionization mass spectrometry (ESI-MS) was performed on an Agilent 1200 high-performance liquid chromatography (HPLC)-mass selective detector mass spectrometer and high-resolution ESI-MS on an Applied Biosystems Q-STAR Elite ESI-LC-MS/MS mass spectrometer. ¹H NMR spectra were performed on a Bruker AV-400 spectrometer at 400 MHz or a Bruker AV-500 spectrometer at 500 MHz. ¹³C NMR spectra were performed on a Bruker AV-500 spectrometer at 125 MHz. Coupling constants (*J*) were expressed in hertz (Hz). Chemical

shifts (δ) of NMR were reported in parts per million units relative to an internal standard (tetramethylsilane). Purity of the compounds was determined by reverse-phase high-performance liquid chromatography (HPLC) analysis to be >95%. HPLC instrument: Dionex Summit HPLC (column: Diamonsil C18, 5.0 μ m, 4.6 \times 250 mm² (Dikma Technologies); detector: PDA-100 photodiode array; injector: ASI-100 autoinjector; pump: p-680A). A flow rate of 1.0 mL/min was used with mobile phase of MeOH in H₂O with a 0.1% modifier (ammonia, v/v).

***N*-(3-(4-Methyl-1*H*-imidazol-1-yl)-5-(trifluoromethyl)phenyl)-2-(pyrimidin-5-yl)isoindoline-5-carboxamide (7a).** To a solution of methyl 2-(pyrimidin-5-yl)isoindoline-5-carboxylate 38 (32 mg, 0.12 mmol) and 3-(4-methyl-1*H*-imidazol-1-yl)-5-(trifluoromethyl)aniline (30 mg, 0.12 mmol) in tetrahydrofuran (THF) (1 mL) was added *t*-BuOK (42 mg, 0.36 mmol) at -20 °C. The mixture was stirred at rt overnight. Then, the reaction mixture was poured into ice-water and extracted with ethyl acetate three times. The combined organic layer was washed with brine, dried over Na₂SO₄, concentrated in vacuo, and purified by flash chromatography on silica gel to give 7a (18 mg, 32% yield). ¹H NMR (400 MHz, DMSO-*d*₆) δ 10.73 (s, 1H), 8.57 (s, 1H), 8.30 (s, 3H), 8.21 (s, 1H), 8.17 (s, 1H), 8.05 (s, 1H), 7.99 (d, *J* = 8.0 Hz, 1H), 7.74 (s, 1H), 7.62 (d, *J* = 8.0 Hz, 1H), 7.49 (s, 1H), 4.79 (s, 4H), 2.19 (s, 3H). ¹³C NMR (125 MHz, DMSO-*d*₆) δ 165.69, 146.85, 141.30, 141.27, 140.51, 139.74, 138.89, 137.91, 137.53, 134.93, 133.42, 130.84 (q, *J* = 32.1 Hz), 129.60, 127.24, 123.61 (q, *J* = 271.3 Hz), 122.88, 122.09, 114.93, 114.19, 111.63, 52.73, 52.59, 13.50. High-resolution mass spectrometry (HRMS) (ESI) [M + H]⁺, calcd: 465.1645, found: 465.1642. HPLC analysis: MeOH/H₂O (70:30), 4.32 min, 96.7% purity.

***N*-(3-(4-Methyl-1*H*-imidazol-1-yl)-5-(trifluoromethyl)phenyl)-2-(pyrimidin-5-ylmethyl)isoindoline-5-carboxamide (7b).** Compound 7b was prepared by following a similar procedure to that for 7a. Yield, 39%. ¹H NMR (500 MHz, CDCl₃) δ 9.15 (s, 1H), 8.88 (s, 1H), 8.77 (s, 2H), 8.18 (s, 1H), 7.79 (s, 1H), 7.78–7.76 (m, 3H), 7.33 (s, 1H), 7.29 (d, *J* = 7.6 Hz, 1H), 7.06 (s, 1H), 3.99 (d, *J* = 6.5 Hz, 4H), 3.95 (s, 2H), 2.25 (s, 3H). ¹³C NMR (125 MHz, CDCl₃) δ 166.26, 158.14, 157.26, 144.70, 140.89, 140.68, 140.29, 138.64, 134.66, 133.27, 133.09 (q, *J* = 32.9 Hz), 132.20, 126.47, 123.34 (q, *J* = 271.5 Hz), 122.89, 121.71, 115.52, 115.14, 114.65, 113.06, 58.89, 58.75, 55.01, 13.69. HRMS (ESI) [M + H]⁺, calcd: 479.1802, found: 479.1802. HPLC analysis: MeOH/H₂O (80:20), 7.72 min, 97.3% purity.

***R*-(3-(4-Methyl-1*H*-imidazol-1-yl)-5-(trifluoromethyl)phenyl)-2-(pyrimidin-5-ylamino)-2,3-dihydro-1*H*-indene-5-carboxamide (7c).** To a solution of methyl (*R*)-2-(pyrimidin-5-ylamino)-2,3-dihydro-1*H*-indene-5-carboxylate 25 (50 mg, 0.19 mmol) and 3-(4-methyl-1*H*-imidazol-1-yl)-5-(trifluoromethyl)aniline (45 mg, 0.19 mmol) in dry THF (1 mL) was added *t*-BuOK (64 mg, 0.56 mmol) at -20 °C. The mixture was stirred overnight at rt. Ice-water was added to the mixture, and then the solution was extracted with ethyl acetate three times. The combined organic layer was washed with brine, dried over Na₂SO₄, concentrated in vacuo, and purified by flash chromatography on silica gel to give the title compound 7c (31 mg, 34%). [α]_D²⁰ -23.1 (c 0.156, MeOH). ¹H NMR (400 MHz, DMSO-*d*₆) δ 10.60 (s, 1H), 8.42 (s, 1H), 8.30 (s, 1H), 8.19 (s, 3H), 8.17 (s, 1H), 7.89 (s, 1H), 7.84 (d, *J* = 7.8 Hz, 1H), 7.72 (s, 1H), 7.48 (s, 1H), 7.44 (d, *J* = 7.9 Hz, 1H), 6.46 (d, *J* = 6.8 Hz, 1H), 4.41–4.34 (m, 1H), 3.46–3.40 (m, 2H), 2.93–2.86 (m, 2H), 2.18 (s, 3H). ¹³C NMR (125 MHz, CDCl₃) δ 166.43, 148.74, 146.03, 141.97, 141.34, 141.06, 140.69, 140.27, 138.64, 134.62, 133.20, 133.08 (q, *J* = 30.4 Hz), 126.43, 125.52, 124.20, 123.33 (q, *J* = 271.2 Hz), 115.48, 115.08, 114.63, 113.06, 53.63, 40.12, 39.91, 13.69. HRMS (ESI) [M + H]⁺, calcd: 479.1802, found: 479.1798. HPLC analysis: MeOH/H₂O (70:30), 4.06 min, 100.0% purity.

***S*-(3-(4-Methyl-1*H*-imidazol-1-yl)-5-(trifluoromethyl)phenyl)-2-(pyrimidin-5-ylamino)-2,3-dihydro-1*H*-indene-5-carboxamide (7d).** Compound 7d was prepared by following a similar procedure as that of 7c. Yield, 60%. [α]_D²⁰ +21.1 (c 0.152, MeOH). ¹H NMR (400 MHz, DMSO-*d*₆) δ 10.61 (s, 1H), 8.42 (s,

1H), 8.30 (s, 1H), 8.20–8.19 (m, 3H), 8.17 (s, 1H), 7.84 (d, *J* = 7.8 Hz, 1H), 7.72 (s, 1H), 7.48 (s, 1H), 7.44 (d, *J* = 7.9 Hz, 1H), 6.46 (d, *J* = 6.8 Hz, 1H), 4.41–4.35 (m, 1H), 3.46–3.40 (m, 2H), 2.93–2.86 (m, 2H), 2.18 (s, 3H), 1.91 (s, 3H). ¹³C NMR (125 MHz, CDCl₃) δ 166.58, 148.56, 146.00, 141.91, 141.26, 141.14, 140.80, 140.13, 138.49, 134.61, 133.17, 133.01 (q, *J* = 32.7 Hz), 126.50, 125.43, 124.24, 123.34 (q, *J* = 271.3 Hz), 115.50, 115.23, 114.64, 112.95, 53.57, 40.07, 39.85, 13.63. HRMS (ESI) [M + H]⁺, calcd: 479.1802, found: 479.1798. HPLC analysis: MeOH/H₂O (80:20), 5.49 min, 97.0% purity.

2-Methyl-*N*-(3-(4-methyl-1*H*-imidazol-1-yl)-5-(trifluoromethyl)phenyl)-2-(pyrimidin-5-ylamino)-2,3-dihydro-1*H*-indene-5-carboxamide (7e). Compound 7e was prepared by following a similar procedure as that of 7c. Yield, 35%. ¹H NMR (500 MHz, CDCl₃) δ 9.02 (s, 1H), 8.56 (s, 1H), 8.18 (s, 1H), 8.04 (s, 2H), 7.77 (s, 2H), 7.71 (d, *J* = 9.2 Hz, 1H), 7.33 (s, 1H), 7.28 (d, *J* = 7.9 Hz, 1H), 7.04 (s, 1H), 4.34 (s, 1H), 3.41–3.32 (m, 2H), 3.08–3.01 (m, 2H), 2.25 (s, 3H), 1.57 (s, 3H). ¹³C NMR (125 MHz, CDCl₃) δ 166.72, 148.18, 145.92, 142.33, 141.72, 140.84, 140.25, 140.12, 138.47, 134.58, 132.95 (q, *J* = 33.0 Hz), 126.57, 125.41, 124.20, 123.32 (q, *J* = 271.0 Hz), 115.51, 115.22, 114.62, 112.91, 61.49, 45.49, 45.35, 27.56, 13.60. HRMS (ESI) [M + H]⁺, calcd: 479.1802, found: 479.1798. HPLC analysis: MeOH/H₂O (80:20), 8.17 min, 100.0% purity.

***R*-(2-(Methyl(pyrimidin-5-yl)amino)-*N*-(3-(4-methyl-1*H*-imidazol-1-yl)-5-(trifluoromethyl)phenyl)-2,3-dihydro-1*H*-indene-5-carboxamide (7f).** Compound 7f was prepared by following a similar procedure as that of 7c. Yield, 71%. [α]_D²⁵ +21.64 (c 0.102, MeOH). ¹H NMR (400 MHz, CDCl₃) δ 9.08 (s, 1H), 8.59 (s, 1H), 8.29 (s, 2H), 8.23 (s, 1H), 7.81 (s, 1H), 7.79–7.76 (m, 3H), 7.35–7.33 (m, 2H), 7.07 (s, 1H), 4.81–4.74 (m, 1H), 3.34–3.23 (m, 2H), 3.14–3.06 (m, 2H), 2.78 (s, 3H), 2.25 (s, 3H). ¹³C NMR (125 MHz, CDCl₃) δ 166.37, 148.15, 146.11, 143.32, 142.05, 141.78, 140.75, 140.28, 138.62, 134.65, 133.19, 133.05 (q, *J* = 33.1 Hz), 126.38, 125.05, 123.81, 123.34 (q, *J* = 271.3 Hz), 115.48, 115.09, 114.63, 112.94, 58.39, 36.29, 36.04, 32.02, 13.69. HRMS (ESI) [M + H]⁺, calcd: 493.1958, found: 493.1954. HPLC analysis: MeOH/H₂O (70:30), 4.75 min, 99.7% purity.

***R*-(2-(Ethyl(pyrimidin-5-yl)amino)-*N*-(3-(4-methyl-1*H*-imidazol-1-yl)-5-(trifluoromethyl)phenyl)-2,3-dihydro-1*H*-indene-5-carboxamide (7g).** Compound 7g was prepared by following a similar procedure as that of 7c. Yield, 35%. [α]_D²⁵ +7.3 (c 0.11, MeOH). ¹H NMR (400 MHz, CDCl₃) δ 8.60 (s, 1H), 8.40 (s, 1H), 8.26 (s, 2H), 8.23 (s, 1H), 7.83 (s, 1H), 7.79 (s, 1H), 7.75–7.73 (m, 2H), 7.38–7.36 (m, 2H), 7.09 (s, 1H), 4.75–4.67 (s, 1H), 3.40–3.31 (m, 4H), 3.17–3.11 (m, 2H), 2.29 (s, 3H), 1.17 (t, *J* = 7.0 Hz, 1H). ¹³C NMR (125 MHz, CDCl₃) δ 166.47, 147.68, 145.90, 141.80, 141.61, 141.57, 140.81, 140.25, 138.58, 134.63, 133.22, 133.02 (q, *J* = 33.2 Hz), 126.48, 125.12, 123.93, 123.34 (q, *J* = 271.2 Hz), 115.48, 115.10, 114.62, 112.89, 58.61, 41.03, 36.68, 36.40, 13.69. HRMS (ESI) [M + H]⁺, calcd: 507.2115, found: 507.2110. HPLC analysis: MeOH/H₂O (70:30), 5.43 min, 99.0% purity.

***R*-(3-(4-Methyl-1*H*-imidazol-1-yl)-5-(trifluoromethyl)phenyl)-2-(propyl(pyrimidin-5-yl)amino)-2,3-dihydro-1*H*-indene-5-carboxamide (7h).** Compound 7h was prepared by following a similar procedure as that of 7c. Yield, 11%. [α]_D²⁵ +1.4 (c 0.146, MeOH). ¹H NMR (500 MHz, CDCl₃) δ 9.39 (s, 1H), 8.49 (s, 1H), 8.16 (s, 1H), 8.14 (s, 2H), 7.79 (s, 1H), 7.75 (s, 1H), 7.73–7.71 (m, 2H), 7.23 (d, *J* = 10.2 Hz, 1H), 7.00 (s, 1H), 4.63–4.57 (m, 1H), 3.26–3.20 (m, 2H), 3.18–3.14 (m, 2H), 3.08–3.00 (m, 2H), 2.19 (s, 3H). ¹³C NMR (125 MHz, CDCl₃) δ 166.59, 147.54, 145.75, 141.83, 141.63, 140.98, 140.11, 138.45, 134.63, 133.25, 132.95 (q, *J* = 33.1 Hz), 126.58, 125.04, 124.03, 123.36 (q, *J* = 271.1 Hz), 115.53, 115.27, 114.64, 112.79, 59.11, 48.78, 36.46, 36.19, 21.50, 13.60, 11.25. HRMS (ESI) [M + H]⁺, calcd: 521.2271, found: 521.2269. HPLC analysis: MeOH/H₂O (70:30), 6.62 min, 98.0% purity.

***R*-(2-(Methyl(pyrimidin-5-yl)amino)-*N*-(3-methyl-5-(4-methyl-1*H*-imidazol-1-yl)phenyl)-2,3-dihydro-1*H*-indene-5-carboxamide (7i).** To a solution of (*R*)-2-(methyl(pyrimidin-5-yl)amino)-2,3-dihydro-1*H*-indole-5-carboxylic acid 30 (100 mg, 0.37 mmol) in 2 mL of CH₂Cl₂ were added 3-(adamantan-1-yl)-5-(4-

methyl-1*H*-imidazol-1-yl)phenylamine (82.2 mg, 0.44 mmol), *O*-(7-azabenzotriazol-1-yl)-*N,N,N',N'*-tetramethyluronium hexafluorophosphate (211 mg, 0.56 mmol), and *N,N*-diisopropylethylamine (0.2 mL, 1.11 mmol). The mixture was stirred overnight at room temperature and diluted with CH₂Cl₂. The resulting solution was washed with water and brine, dried over Na₂SO₄, concentrated in vacuo, and purified by column chromatography to give compound 7i. (51 mg, 32% yield). [α]_D²⁵ +21.9 (c 0.082, MeOH). ¹H NMR (400 MHz, CDCl₃) δ 8.64 (s, 1H), 8.33 (s, 3H), 8.10 (s, 1H), 7.95 (s, 1H), 7.81 (s, 1H), 7.79 (s, 1H), 7.74 (d, *J* = 7.7 Hz, 1H), 7.40 (s, 1H), 7.36 (d, *J* = 7.8 Hz, 1H), 7.08 (s, 1H), 6.97 (s, 1H), 4.84–4.78 (m, 1H), 3.36–3.30 (m, 2H), 3.16–3.10 (m, 2H), 2.80 (s, 3H), 2.42 (s, 3H), 2.32 (s, 3H). ¹³C NMR (125 MHz, CDCl₃) δ 166.14, 148.12, 145.61, 143.33, 141.92, 141.75, 140.84, 139.61, 137.97, 133.80, 126.24, 124.92, 123.70, 119.29, 117.46, 114.77, 110.22, 58.33, 36.29, 36.07, 31.96, 21.70, 13.68. HRMS (ESI) [*M* + *H*]⁺, calcd: 439.2241, Found: 439.2239. HPLC analysis: MeOH/H₂O (70:30), 3.82 min, 99.6% purity.

(*R*)-*N*-(3-Ethyl-5-(4-methyl-1*H*-imidazol-1-yl)phenyl)-2-(methyl(pyrimidin-5-yl)amino)-2,3-dihydro-1*H*-indene-5-carboxamide (7j). Compound 7j was prepared by following a similar procedure as that of 7i. Yield, 54%. [α]_D²⁵ +24.5 (c 0.1098, MeOH). ¹H NMR (400 MHz, CDCl₃) δ 8.64 (s, 1H), 8.34 (s, 2H), 8.05 (s, 1H), 7.97 (s, 1H), 7.85 (s, 1H), 7.81 (s, 1H), 7.74 (d, *J* = 7.7 Hz, 1H), 7.38–7.36 (m, 1H), 7.09 (s, 1H), 6.99 (s, 1H), 4.86–4.79 (m, 1H), 3.37–3.31 (m, 2H), 3.17–3.10 (m, 2H), 2.81 (s, 3H), 2.72 (q, *J* = 7.6 Hz, 2H), 2.34 (s, 3H), 1.29 (t, *J* = 7.6 Hz, 3H). ¹³C NMR (125 MHz, CDCl₃) δ 166.11, 148.15, 147.20, 145.63, 143.34, 141.96, 141.86, 139.56, 138.16, 134.71, 133.84, 126.21, 124.95, 123.68, 118.07, 116.42, 114.83, 110.50, 58.40, 36.30, 36.09, 31.97, 29.02, 18.57, 15.41, 13.76. HRMS (ESI) [*M* + *H*]⁺, calcd: 453.2397, found: 453.2398. HPLC analysis: MeOH/H₂O (70:30), 4.34 min, 98.1% purity.

(*R*)-*N*-(3-Isopropyl-5-(4-methyl-1*H*-imidazol-1-yl)phenyl)-2-(methyl(pyrimidin-5-yl)amino)-2,3-dihydro-1*H*-indene-5-carboxamide (7k). Compound 7k was prepared by following a similar procedure as that of 7i. Yield, 19%. [α]_D²⁵ +21.0 (c 0.114, MeOH). ¹H NMR (500 MHz, CDCl₃) δ 8.62 (s, 1H), 8.43 (d, *J* = 8.4 Hz, 1H), 8.31 (s, 2H), 7.80 (s, 2H), 7.77–7.75 (m, 2H), 7.39 (s, 1H), 7.34 (d, *J* = 7.8 Hz, 1H), 7.05 (s, 1H), 6.98 (s, 1H), 4.82–4.76 (m, 1H), 3.33–3.28 (m, 2H), 3.13–3.08 (m, 2H), 2.97–2.92 (m, 1H), 2.78 (s, 3H), 2.27 (s, 3H), 1.28 (d, *J* = 6.9 Hz, 6H). ¹³C NMR (125 MHz, CDCl₃) δ 166.10, 152.00, 148.16, 145.64, 143.36, 141.97, 141.87, 139.70, 138.07, 133.82, 126.23, 124.96, 123.69, 116.87, 115.11, 110.76, 58.35, 36.31, 36.10, 34.41, 31.96, 23.92, 13.64. HRMS (ESI) [*M* + *H*]⁺, calcd: 467.2554, found: 467.2558. HPLC analysis: MeOH/H₂O (80:20), 8.54 min, 95.7% purity.

(*R*)-*N*-(3-(*tert*-Butyl)-5-(4-methyl-1*H*-imidazol-1-yl)phenyl)-2-(methyl(pyrimidin-5-yl)amino)-2,3-dihydro-1*H*-indene-5-carboxamide (7l). Compound 7l was prepared by following a similar procedure as that of 7i. Yield, 32%. [α]_D²⁵ +20.5 (c 0.078, MeOH). ¹H NMR (400 MHz, CDCl₃) δ 8.62 (s, 1H), 8.32 (s, 1H), 8.21 (s, 1H), 8.14 (s, 1H), 7.85 (s, 1H), 7.83–7.79 (m, 2H), 7.74 (s, 1H), 7.36 (d, *J* = 7.6 Hz, 1H), 7.15 (s, 2H), 4.85–4.80 (m, 1H), 3.39–3.28 (m, 2H), 3.19–3.07 (m, 2H), 2.79 (s, 3H), 2.38 (s, 3H), 1.38 (s, 9H). ¹³C NMR (125 MHz, CDCl₃) δ 166.18, 154.47, 148.02, 145.60, 143.38, 141.98, 141.71, 139.63, 133.70, 126.33, 124.93, 123.64, 116.38, 114.05, 110.63, 58.51, 58.28, 55.19, 43.23, 36.35, 36.08, 35.28, 31.89, 31.32, 29.83, 18.56, 13.41, 12.44. HRMS (ESI) [*M* + *H*]⁺, calcd: 481.2710, Found: 481.2712. HPLC analysis: MeOH/H₂O (80:20), 10.38 min, 95.3% purity.

(*R*)-*N*-(3-Cyclohexyl-5-(4-methyl-1*H*-imidazol-1-yl)phenyl)-2-(methyl(pyrimidin-5-yl)amino)-2,3-dihydro-1*H*-indene-5-carboxamide (7m). Compound 7m was prepared by following a similar procedure as that of 7i. Yield, 28%. [α]_D²⁵ +23.7 (c 0.076, MeOH). ¹H NMR (400 MHz, DMSO-*d*₆) δ 10.24 (s, 1H), 8.51 (s, 1H), 8.45 (s, 2H), 8.02 (s, 1H), 7.888–7.86 (m, 2H), 7.82 (d, *J* = 7.8 Hz, 2H), 7.62 (s, 1H), 7.42 (d, *J* = 7.9 Hz, 1H), 7.34 (s, 1H), 7.18 (s, 1H), 5.03–4.96 (m, 1H), 3.27–3.25 (m, 2H), 3.12–3.07 (m, 2H), 2.77 (s, 3H), 2.58–2.56 (m, 1H), 2.17 (s, 3H), 1.87–1.71 (m, 5H), 1.51–1.23 (m, 5H). ¹³C NMR (125 MHz, DMSO-*d*₆) δ 165.59,

149.84, 146.93, 145.53, 143.24, 141.61, 141.25, 140.36, 138.27, 137.06, 134.53, 133.09, 126.32, 124.29, 123.56, 116.56, 114.27, 113.96, 109.66, 57.26, 43.84, 35.18, 35.02, 33.70, 31.09, 26.22, 25.55, 13.52. HRMS (ESI) [*M* + *H*]⁺, calcd: 507.2867, Found: 507.2872. HPLC analysis: MeOH/H₂O (80:20), 22.43 min, 96.3% purity.

(*R*)-*N*-(3-(Adamantan-1-yl)-5-(4-methyl-1*H*-imidazol-1-yl)phenyl)-2-(methyl(pyrimidin-5-yl)amino)-2,3-dihydro-1*H*-indene-5-carboxamide (7n). Compound 7n was prepared by following a similar procedure as that of 7i. (90 mg, 25%). [α]_D²⁵ +5 (c 0.1, MeOH). ¹H NMR (400 MHz, CDCl₃) δ 8.62 (s, 1H), 8.45 (s, 1H), 8.32 (s, 2H), 7.88 (s, 1H), 7.78 (d, *J* = 7.8 Hz, 1H), 7.56 (s, 1H), 7.34 (d, *J* = 7.8 Hz, 1H), 7.10 (s, 1H), 7.07 (s, 1H), 4.83–4.76 (m, 1H), 3.34–3.28 (m, 2H), 3.14–3.08 (m, 2H), 2.79 (s, 3H), 2.30 (s, 3H), 2.11 (s, 3H), 1.92 (s, 6H), 1.82–1.73 (m, 6H). ¹³C NMR (125 MHz, CDCl₃) δ 166.17, 154.58, 148.14, 145.53, 143.36, 139.70, 137.73, 134.59, 133.81, 126.36, 124.87, 123.76, 116.05, 115.24, 113.85, 110.82, 58.37, 43.22, 36.76, 36.72, 36.27, 36.05, 31.96, 28.94. HRMS (ESI) [*M* + *H*]⁺, calcd: 559.3180, found: 559.3183. HPLC analysis: MeOH/H₂O (80:20), 20.76 min, 100.0% purity.

***tert*-Butyl (*R*)-(5-Bromo-2,3-dihydro-1*H*-inden-2-yl)-carbamate (10).** To a mixture of (*R*)-5-bromo-2,3-dihydro-1*H*-inden-2-amine 8 (40 mg, 0.19 mmol) and Et₃N (39 μ L, 0.28 mmol) in 1 mL of dichloromethane (DCM) was added (Boc)₂O (131 μ L, 0.57 mmol). The reaction mixture was stirred at room temperature overnight. The mixture was then poured into water and extracted three times with dichloromethane. The combined organic phase was dried over Na₂SO₄ and purified by column chromatography to give 10 (53 mg, 90%). ¹H NMR (400 MHz, DMSO-*d*₆) δ 7.38 (s, 1H), 7.29 (d, *J* = 8.0 Hz, 1H), 7.17 (s, 1H), 7.14 (d, *J* = 8.0 Hz, 1H), 4.22–4.17 (m, 1H), 3.14–3.02 (m, 2H), 2.79–2.68 (m, 2H), 1.38 (s, 9H). MS (ESI) *m/z* 335.3 [*M* + *Na*]⁺.

***tert*-Butyl (*R*)-(5-Bromo-2,3-dihydro-1*H*-inden-2-yl)-carbamate (12).** *tert*-Butyl (*R*)-(5-bromo-2,3-dihydro-1*H*-inden-2-yl)carbamate 10 (600 mg, 1.92 mmol) was dissolved in 2 mL of DMF, and sodium hydride (89 mg, 2.22 mmol, in 60% mineral oil) was added. The reaction was stirred for 40 min, and then CH₃I (0.13 mL, 2.12 mmol) was added dropwise in an ice bath. The reaction was stirred overnight at room temperature. The mixture was quenched by water and extracted with ethyl acetate three times. The combined organic layer was dried over magnesium sulfate, filtered, evaporated, and purified by silica gel column chromatography to give 12 (501 mg, 80%). ¹H NMR (500 MHz, DMSO-*d*₆) δ 7.41 (s, 1H), 7.32 (d, *J* = 1.6 Hz, 1H), 7.31 (d, *J* = 1.5 Hz, 1H), 7.17 (d, *J* = 8.0 Hz, 1H), 4.85 (s, 1H), 3.09–2.99 (m, 2H), 2.96–2.85 (m, 2H), 2.64 (s, 3H), 1.39 (s, 9H). MS (ESI) *m/z* 348.3 [*M* + *Na*]⁺.

Methyl (*R*)-2-((*tert*-Butoxycarbonyl)amino)-2,3-dihydro-1*H*-indene-5-carboxylate (15). A mixture of *tert*-butyl (*R*)-(5-bromo-2,3-dihydro-1*H*-inden-2-yl)carbamate 10 (100 mg, 0.32 mmol), Pd(OAc)₂ (3.6 mg, 0.016 mmol), MeOH, DMF, and triethylamine (89 μ L, 0.64 mmol) was stirred overnight at 100 °C under carbon monoxide. The solids were filtered off, and the filtrate was concentrated under vacuo. The residue was purified by column chromatography to give 15 (55 mg, 59%). ¹H NMR (500 MHz, DMSO-*d*₆) δ 7.77 (s, 1H), 7.75 (s, 1H), 7.32 (d, *J* = 7.5 Hz, 1H), 7.18 (d, *J* = 6.5 Hz, 1H), 4.26–4.22 (m, 1H), 3.82 (s, 3H), 3.19–3.14 (m, 2H), 2.84–2.78 (m, 2H), 1.39 (s, 9H). MS (ESI) *m/z* 314.6 [*M* + *Na*]⁺.

Methyl (*R*)-2-((*tert*-Butoxycarbonyl)(methyl)amino)-2,3-dihydro-1*H*-indene-5-carboxylate (17). A mixture of *tert*-butyl (*R*)-(5-bromo-2,3-dihydro-1*H*-inden-2-yl)(methyl)carbamate 12 (2.39 g, 7.35 mmol), PdCl₂dppf (548 mg, 0.7 mmol), MeOH (6 mL), DMF (35 mL), and triethylamine (3.1 mL, 22 mmol) was stirred overnight at 100 °C under carbon monoxide. The solids were filtered off, and the filtrate was concentrated under vacuo. The residue was purified by column chromatography to give 17 (1.9 g, 85%). ¹H NMR (500 MHz, DMSO-*d*₆) δ 7.80 (s, 1H), 7.77 (d, *J* = 7.8 Hz, 1H), 7.35 (d, *J* = 7.9 Hz, 1H), 4.90 (s, 1H), 3.83 (s, 3H), 3.17–3.10 (m, 2H), 3.02–2.96 (m, 2H), 2.65 (s, 3H), 1.39 (s, 9H).

Methyl (*R*)-2-Amino-2,3-dihydro-1*H*-indene-5-carboxylate Hydrochloride (20). A mixture of methyl (*R*)-2-((*tert*-

butoxycarbonyl)amino)-2,3-dihydro-1H-indene-5-carboxylate **15** (126 mg, 0.43 mmol) and 4 M HCl (1 mL) in dioxane (1 mL) was stirred at 60 °C for 2 h. The reaction mixture was concentrated to give the amine, which was used directly for the next step without further purification. MS (ESI) m/z 192.2 $[M + H]^+$.

Methyl (R)-2-(Methylamino)-2,3-dihydro-1H-indene-5-carboxylate (22). A mixture of methyl (R)-2-((*tert*-butoxycarbonyl)-(methyl)amino)-2,3-dihydro-1H-indene-5-carboxylate **17** (1.9 g, 6.22 mmol) and 4 M HCl (13 mL) in dioxane (13 mL) was stirred at 50 °C for 4 h. The solvent was evaporated in vacuum. The residue was diluted with H₂O and extracted with dichloromethane three times. The combined organic phase was washed with saturated NaHCO₃. The aqueous layer was extracted twice with dichloromethane. The combined organic layer was washed with brine and dried over anhydrous Na₂SO₄. The solvent was evaporated in vacuo to give the free amine **22** (1.0 g, 78%), which was used directly in the next step without further purification.

Methyl (R)-2-(Pyrimidin-5-ylamino)-2,3-dihydro-1H-indene-5-carboxylate (25). A sealed tube containing methyl (R)-2-amino-2,3-dihydro-1H-indene-5-carboxylate hydrochloride **20** (630 mg, 2.77 mmol), 5-bromopyrimidine (656 mg, 4.1 mmol), Pd(dba)₂ (10 mmol %), Ruphos (20 mmol %), and Cs₂CO₃ (2.7 g, 8.31 mmol) in toluene was flushed with argon and then heated overnight at 80 °C. The reaction mixture was cooled to room temperature, filtered, concentrated in vacuo, and purified by flash column to obtain **25** (450 mg, 60%). ¹H NMR (400 MHz, DMSO-*d*₆) δ 8.41 (s, 1H), 8.17 (s, 2H), 7.83 (s, 1H), 7.79 (d, J = 7.6 Hz, 1H), 7.39 (d, J = 8.0 Hz, 1H), 6.44 (d, J = 6.4 Hz, 1H), 4.36–4.30 (m, 1H), 3.83 (s, 3H), 3.42–3.37 (m, 2H), 2.88–2.83 (m, 2H). MS (ESI) m/z 270.3 $[M + H]^+$.

Methyl (R)-2-(Methyl(pyrimidin-5-yl)amino)-2,3-dihydro-1H-indene-5-carboxylate (27). A sealed tube containing methyl (R)-2-(methylamino)-2,3-dihydro-1H-indene-5-carboxylate **22** (500 mg, 2.4 mmol), 5-bromopyrimidine (578 mg, 3.6 mmol), Pd(dba)₂ (10 mmol %), Ruphos (20 mmol %), and Cs₂CO₃ (1.6 g, 4.8 mmol) in toluene was flushed with argon and then heated overnight at 80 °C. The reaction mixture was cooled to room temperature, filtered, concentrated in vacuo, and purified by flash column to give **27** (382 mg, 56%). ¹H NMR (400 MHz, DMSO-*d*₆) δ 8.50 (s, 1H), 8.43 (s, 2H), 7.84 (s, 1H), 7.80 (d, J = 7.9 Hz, 1H), 7.39 (d, J = 7.9 Hz, 1H), 5.00–4.93 (m, 1H), 3.83 (s, 3H), 3.29–3.22 (m, 2H), 3.10–3.03 (m, 2H), 2.74 (s, 3H). MS (ESI) m/z 284.3 $[M + H]^+$.

(R)-2-(Methyl(pyrimidin-5-yl)amino)-2,3-dihydro-1H-indene-5-carboxylic Acid (30). To a solution of methyl (R)-2-(methyl(pyrimidin-5-yl)amino)-2,3-dihydro-1H-indene-5-carboxylate **27** (1 g, 3.5 mmol) in dioxane was added 1 M sodium hydroxide solution. The reaction mixture was stirred at 50 °C overnight. The solvent was evaporated under vacuo, and the resulting residue was dissolved in water. The solution was acidified to pH 4, and a white precipitate was formed, which was collected, washed with water, and dried to give **30** (772.9 mg, 82%). ¹H NMR (400 MHz, DMSO-*d*₆) δ 12.78 (s, 1H), 8.50 (s, 1H), 8.43 (s, 2H), 7.82 (s, 1H), 7.78 (d, J = 7.6 Hz, 1H), 7.36 (d, J = 8.0 Hz, 1H), 5.09–4.89 (m, 1H), 3.25 (dd, J = 17.6, 8.0 Hz, 2H), 3.12–2.98 (m, 2H), 2.74 (s, 3H).

Compounds **33**–**37** were prepared according to the published methods.³⁶

5-Bromoisindoline-1,3-dione (33). 4-bromophthalic anhydride **32** (1 g, 4.4 mmol) and formamide were combined in a sealed tube. The reaction mixture was stirred overnight at 200 °C. After cooling to room temperature, 10 mL of water was added to the reaction mixture. The precipitate was filtered, washed with methanol, and dried in a vacuum oven to give **33** (788 mg, 79%). ¹H NMR (500 MHz, DMSO-*d*₆) δ 11.46 (s, 1H), 8.04–8.00 (m, 1H), 8.01 (d, J = 3.0 Hz, 1H), 7.75 (d, J = 8.0 Hz, 1H). MS (ESI) m/z 247.2 $[M + Na]^+$.

5-Bromoisindoline (34). To a solution of 5-bromoisindoline-1,3-dione **33** (788 mg, 3.5 mmol) in THF (20 mL) was added the brane-THF complex (1 M, 14 mL). The reaction was heated to reflux overnight. After cooling to room temperature, the solvent was concentrated in vacuo. Water was added to the residue. The aqueous

phase was extracted with DCM three times. The combined organic phase was dried over Na₂SO₄, filtered, and concentrated in vacuo to give **34** (282 mg, 41%), which was used for the next step without further purification. MS (ESI) m/z 198.4 $[M + H]^+$.

***tert*-Butyl 5-Bromoisindoline-2-carboxylate (35).** To 5-bromoisindoline **34** (282 mg, 1.42 mmol) in 6 mL of THF were added (Boc)₂O (1 mL, 4.3 mmol) and NaHCO₃ (360.8 mg, 4.29 mmol). The reaction mixture was stirred at room temperature overnight. The reaction was quenched by water and extracted three times with CH₂Cl₂. The combined organic phase was washed with brine, dried over Na₂SO₄, concentrated in vacuo, and purified by silica gel column chromatography to give **35** (238 mg, 56%). ¹H NMR (400 MHz, DMSO-*d*₆) δ 7.55 (d, J = 4.4 Hz, 1H), 7.46 (d, J = 8.0 Hz, 1H), 7.28 (dd, J = 8.0, 4.0 Hz, 1H), 4.55 (dd, J = 14.8, 9.2 Hz, 4H), 1.45 (s, 9H). MS (ESI) m/z 320.3 $[M + Na]^+$.

2-(*tert*-Butyl) 5-Methyl Isoindoline-2,5-dicarboxylate (36). A mixture of *tert*-butyl-5-bromoisindoline-2-carboxylate **35** (238 mg, 0.8 mmol), Pd(dppf)Cl₂-CH₂Cl₂ (66 mg, 0.08 mmol), MeOH (1 mL), DMF (4 mL), and triethylamine (0.3 mL, 2.4 mmol) was stirred overnight at 100 °C under carbon monoxide. The solids were filtered off, and the filtrate was concentrated under vacuo. The residue was purified by column chromatography to give **36** (159 mg, 72%). ¹H NMR (400 MHz, DMSO-*d*₆) δ 7.90 (dd, J = 12.4, 8.8 Hz, 2H), 7.47 (dd, J = 7.6, 4.8 Hz, 1H), 4.63 (d, J = 2.8 Hz, 4H), 3.85 (s, 3H), 1.46 (s, 9H).

Methyl Isoindoline-5-carboxylate Hydrochloride (37). 2-(*tert*-Butyl) 5-methylisoindoline-2,5-dicarboxylate **36** (154 mg, 0.2 mmol) was stirred in a mixture of 4 M HCl (1.5 mL) and dioxane (1.5 mL) at 50 °C for 4 h. The reaction mixture was concentrated in vacuo to give **37**, which was used directly for the next step without further purification. MS (ESI) m/z 178.1 $[M + H]^+$.

Methyl 2-(Pyrimidin-5-yl)isoindoline-5-carboxylate (38). 5-Bromopyrimidine (93.6 mg, 0.59 mmol), Pd(dba)₂ (10 mmol %), Ruphos (20 mmol %), Cs₂CO₃ (703.8 mg, 2.16 mmol), methyl isoindoline-5-carboxylate hydrochloride **37** (115 mg, 0.54 mmol), and toluene (3 mL) were combined in a sealed tube. The vessel was evacuated and replaced with argon. The reaction was stirred overnight at 80 °C. After cooling to room temperature, the reaction mixture was filtered, and the filtrate was concentration in vacuo and purified by flash column to afford **38** (40 mg, 29%). ¹H NMR (400 MHz, DMSO-*d*₆) δ 8.55 (s, 1H), 8.25 (s, 2H), 7.99 (s, 1H), 7.95 (d, J = 8.0 Hz, 1H), 7.56 (d, J = 8.0 Hz, 1H), 4.76 (d, J = 3.2 Hz, 4H), 3.87 (s, 3H). MS (ESI) m/z 256.2 $[M + H]^+$.

Methyl 2-(Pyrimidin-5-ylmethyl)isoindoline-5-carboxylate (39). To methyl isoindoline-5-carboxylate hydrochloride **37** (90 mg, 0.42 mmol) in DMF were added 5-chloromethylpyrimidine (65 mg, 0.41 mmol) and potassium carbonate (145 mg, 1.05 mmol). The reaction was stirred overnight at 50 °C. Then, water (10 mL) was added to the reaction mixture and extracted with ethyl acetate three times. The combined organic phase was dried over Na₂SO₄, concentrated in vacuo, and purified by column chromatography to give **39** (44 mg, 41%). ¹H NMR (500 MHz, CDCl₃) δ 9.17 (s, 1H), 8.79 (s, 2H), 7.95–7.90 (m, 1H), 7.87 (s, 1H), 7.25 (s, 1H), 4.00 (s, 4H), 3.95 (s, 2H), 3.90 (s, 3H). MS (ESI) m/z 270.3 $[M + H]^+$.

In Vitro Kinase Assay. Inhibition activity of compounds against TrkA/TrkB/TrkC was determined using the FRET-based Z'-Lyte assay system according to the manufacturer's instructions (Invitrogen). Tyr1 peptide was used as the substrate. The reactions were carried out in 384-well plates in a 10 μ L reaction volume with appropriate amount of kinases in 50 mM *N*-(2-hydroxyethyl)piperazine-*N'*-ethanesulfonic acid (HEPES) (pH 7.5), 10 mM MgCl₂, 1 mM ethylene glycol-bis(β -aminoethyl ether)-*N,N,N',N'*-tetraacetic acid (EGTA), and 0.01% Brij-35. TrkA/TrkB/TrkC kinase reactions were incubated 1.5 h at room temperature in the presence of 2 μ M of substrate with 400, 25, and 50 μ M ATP, respectively, and in the presence of various concentrations of the compounds; then, 5 μ L of the development reagent was added for further 1 h room-temperature incubation followed by the addition of 5 μ L of the stop solution. The fluorescence-to-signal ratio of 400 nm (excitation)/445 nm and 520 nm (emission) was examined with an EnVision

Multilabel Reader (PerkinElmer, Inc.). Data analysis and curve fitting were performed using GraphPad Prism5 (GraphPad Software, Inc.).

The effects of compounds on the kinases DDR1 and DDR2 were assessed using a LanthaScreen Eu kinase activity assay technology (Invitrogen). Kinase reactions are performed in a 10 μ L volume in low-volume 384-well plates. The kinases in the reaction buffer consist of 50 mM HEPES pH 7.5, 0.01% Brij-35, 10 mM MgCl₂, and 1 mM EGTA; the concentration of the fluorescein–poly-GAT substrate (Invitrogen) in the assay is 100 nM. Kinase reactions were initiated with the addition of 100 nM ATP in the presence of serials of dilutions of compounds. The reactions were allowed to proceed for 1 h at room temperature before a 10 μ L preparation of EDTA (20 mM) and Eu-labeled antibody (4 nM) in time-resolved (TR)-FRET dilution buffer are added. The final concentration of antibody in the assay well is 2 nM, and the final concentration of EDTA is 10 mM. The plate is allowed to incubate at room temperature for one more hour before the TR-FRET emission ratios of 665/340 nm were acquired on a PerkinElmer EnVision multilabel reader (Perkin-Elmer, Inc.). Data analysis and curve fitting were performed using GraphPad Prism 7 software.

KINOMEScan. Kinase-tagged T7 phage strains were prepared in an *Escherichia coli* host derived from the BL21 strain. *E. coli* were grown to log-phase and infected with the T7 phage and incubated with shaking at 32 °C until lysis. The lysates were centrifuged and filtered to remove cell debris. The remaining kinases were produced in HEK-293 cells and subsequently tagged with DNA for quantitative polymerase chain reaction (qPCR) detection. Streptavidin-coated magnetic beads were treated with biotinylated small-molecule ligands for 30 min at room temperature to generate affinity resins for kinase assays. The liganded beads were blocked with excess biotin and washed with blocking buffer [SeaBlock (Pierce), 1% bovine serum albumin (BSA), 0.05% Tween 20, 1 mM dithiothreitol (DTT)] to remove the unbound ligand and to reduce nonspecific binding. Binding reactions were assembled by combining kinases, liganded affinity beads, and compound 7i in 1 \times binding buffer [20% SeaBlock, 0.17 \times phosphate-buffered saline (PBS), 0.05% Tween 20, 6 mM DTT]. All reactions were performed in polystyrene 96-well plates in a final volume of 0.135 mL. The assay plates were incubated at room temperature with shaking for 1 h, and the affinity beads were washed with wash buffer (1 \times PBS, 0.05% Tween 20). The beads were then resuspended in an elution buffer (1 \times PBS, 0.05% Tween 20, 0.5 μ M nonbiotinylated affinity ligand) and incubated at room temperature with shaking for 30 min. The kinase concentration in the eluates was measured by qPCR. For primary screening, compound 6j was screened at the concentration of 1 μ M, and the results are reported as “% Ctrl”.

For K_d determination, an 11-point 3-fold serial dilution of compound 7f was prepared in 100% DMSO at 100 \times final test concentration and subsequently diluted to 1 \times in the assay (final DMSO concentration = 1%). Binding constants (K_d values) were calculated with a standard dose–response curve using the Hill equation.

Western Blot Analysis. Pan02, BMF-A3, and CT1A-C11 cells were cultured in DMEM (Corning) containing 10% fetal bovine serum (FBS) and maintained at 37 °C in a humidified incubator with 5% CO₂ and 95% air. For the collagen and 7f treatment, cells were cultured in 10 mL of complete media with 50 μ g/mL collagen and indicated concentration of 7f for 8 or 18 h. Cells were lysed, supernatants were recovered by centrifugation at 13 000 rpm, protein concentration was measured, and equal amounts of total protein were separated by sodium dodecyl sulfate–polyacrylamide gel electrophoresis. Proteins were transferred to poly(vinylidene difluoride) membranes (Bio-Rad, Hercules, CA) followed by blockade for 1 h in 5% bovine serum albumin in TBS-T. Membranes were incubated overnight at 4 °C with primary antibody phospho-DDR1 (Tyr792, Cell Signaling #11994), DDR1 (Santa Cruz SC-532), phospho-PYK2 (Tyr402, Cell Signaling #3291), PYK2 (Cell Signaling #3292), PEAK1 (Millipore 09-274), phospho-PEAK1 (Tyr665, Millipore #ABT52), E-cadherin (24E10, Cell Signaling #3195), N-cadherin (13A9, Cell Signaling #3195), and TUBULIN α (Biorad,

MCA77D800). Membranes were incubated with the corresponding horseradish peroxidase-conjugated secondary antibody (Pierce Biotechnologies, Rockford, IL) for 1 h. Specific bands were detected using the enhanced chemiluminescence reagent (ECL, PerkinElmer Life Sciences, Boston, MA) on an autoradiographic film.

Epithelial–Mesenchymal Transition Assay. For immunofluorescent staining, cells were treated with 50 μ g/mL collagen and indicated concentration of 7f for 24 h. Cells were fixed with methanol and stained with E-cadherin (24E10, Cell Signaling #3195), N-cadherin (13A9, Cell Signaling #3195), and DAPI. Fluorescent images were captured with a Photometric CoolSNAP HQ camera using NIS Elements AR 2.3 Software (Nikon).

For 3D culture, cells were embedded in ECM consisting of 5 mg/mL matrigel (BD Biosciences) and 2.1 mg/mL collagen I (BD Biosciences). Cultures were overlaid with DMEM + 10% FBS containing 2% matrigel. For analysis of spheroid morphology, 48 h after plating onto ECM, cells were fixed with methanol and stained with phalloidin and DAPI. Fluorescent images were captured with a Photometric CoolSNAP HQ camera using NIS Elements AR 2.3 Software (Nikon).

Colony Formation Assay. Cells were cultured in six-well tissue culture plates at low density (1000 cells per well) in 2 mL of media with 10% FBS \pm 7f at the indicated doses for 10 days. A DMSO control was added to the respective wells to demonstrate the vehicle-independent effect. Cells were then stained with crystal violet.

3-(4,5-Dimethylthiazol-2-yl)-2,5-diphenyltetrazolium Bromide Assay. Cells were plated at 2000 cells/well in tissue-culture-treated 96-well plates. The following day, different concentration of 7f was added to each plate in a dilution series across the plate. On day 5, 20 μ L of thiazolyl blue tetrazolium blue was added, followed by a 3 h incubation at 37 °C, and then the medium was removed, and 100 μ L of DMSO was added to each well. The absorbance was read at 540 nm on a plate reader.

Wound-Healing Assay. Cells were cultured in six-well tissue culture plates at high density (~90% confluence) in 2 mL of media with 5% FBS. Uniform scratches were made down the center of each well with a p20 pipette tip, cells were gently washed with PBS to remove the loose cell debris, and drug was added in media containing 5% FBS. Each condition was in triplicates. Images from the center of each well were taken at 0 and 24 h. The wound width (μ m) was measured using NIS Elements AR 2.30 software. The initial wound width was used to verify consistency in scratches.

Determination of Pharmacokinetic Parameters in Rats. All animal studies were performed according to the protocols and guidelines of the institutional care and use committee. The 4–6 week old male Sprague-Dawley rats were purchased from the Shanghai Laboratory Animal Research Center (Shanghai, China). All of the procedures related to animal handling, care, and treatment in this article were performed in compliance with Agreement of the Ethics Committee on Laboratory Animal Care and the Guidelines for the Care and Use of Laboratory Animals in Shanghai, China. Animals were maintained on standard animal chow and water ad libitum, in a climate-controlled room (23 \pm 1 °C, 30–70% relative humidity, a minimum of 10 exchanges of room air/h and a 12 h light/dark cycle) for one week prior to experiments. The compound was dissolved in the solution containing 2% DMSO, 4% ethanol, 4% castor oil, and 90% ddH₂O. Pharmacokinetic properties of SD rats (male) were determined following intravenous (iv) and oral administration. Animals were randomly distributed into two experimental groups ($n = 3$). The oral groups were given 25 mg/kg by gastric gavage. The other group was dosed by injection into the tail vein (5 mg/kg). After a single administration, whole blood samples (100–200 μ L) were obtained from the orbital venous plexus at the following time points after dosing: 5, 10, and 30 min and 1, 2, 3, 4, 6, 8, 11, and 24 h (po); 2, 10, and 30 min and 1, 2, 3, 4, 6, 8, 11, and 24 h (iv). Whole blood samples were collected in heparinized tubes. The plasma fraction was immediately separated by centrifugation (8000 rpm, 6 min, 4 °C) and stored at –20 °C until liquid chromatography–mass spectrometry analysis. The rats were humanely euthanized by carbon dioxide 24 h after experiment without pain. The pharmacokinetics parameters were

calculated by analyzing the compound concentration in plasma samples using the pharmacokinetic software DAS.2.0.

In Vivo Anticancer Activity Assay. All animals were housed in a pathogen-free facility with access to food and water ad libitum. C57BL/6 mice were purchased from the UT Southwestern Mouse Breeding Core. Pan02 and BMF-A3 cells (5×10^5) were injected orthotopically in 6–8 week-old C57BL/6 mice. Fourteen days after tumor cell injection, mice were randomized to receive treatment. Experiments were approved and performed in accordance with the Institutional Animal Care and Use Committee at UT Southwestern. Experiments were stopped after the designated time post tumor cell implantation. Tumors were harvested, and tumor weight was measured. Data sets were analyzed by ANOVA.

Molecular Modeling. All of the procedures were performed in Maestro 11.2 (version 11.2, Schrödinger, LLC, New York, NY, 2017). The DDR1 (PDB code: 5FDP and 6HP9) and TrkC (PDB code: 3V5Q) proteins were processed using the “Protein Preparation Wizard” workflow in Maestro 9.4 (version 11.2, Schrödinger, LLC, New York, NY, 2017) to add bond orders and hydrogens. All hetatm residues and crystal water molecules beyond 5 Å from the het group were removed. Compounds were built by the LigPrep module using the OPLS-2005 force field. The glide module was used as the docking program. The grid-enclosing box was placed on the centroid of the OLI, which was extracted from the crystal structures of DDR1 and TrkC separately. The standard precision approach of Glide was adopted to dock compounds **6** and **7a–n** to DDR1 and compound **7c** to TrkC with the default parameters.

Crystallization and Structure Determination. The kinase domain of human DDR1 (Uniprot Q08345, residues 601–913) was expressed as an N-terminal 6× His fusion in Sf9 cells and purified by nickel affinity chromatography followed by tag cleavage with tobacco etch virus protease and then size exclusion chromatography on an S200 column (GE Healthcare). Protein at 12 mg/mL in 50 mM HEPES pH 7.5, 300 mM NaCl, 0.5 mM tris(2-carboxyethyl)-phosphine, 2% DMSO was incubated with 1 mM compound **7c** for 3 h on ice and then filtered to 0.22 μm. Then, 150 nL of sitting drops was set up with diffracting crystals being obtained from a 1:2 ratio of protein to mother liquor (10% ethylene glycol, 0.2 M sodium sulfate, 25% poly(ethylene glycol) 1500, 0.1 M bis-tris-propane pH 7.1). Crystals were cryoprotected in the mother liquor supplemented with 25% ethylene glycol and flash-frozen in liquid nitrogen. Diffraction was carried out at Diamond Light Source beamline I04 at 100 K. Data were indexed and integrated using XDS³⁷ and scaled using AIMLESS.³⁸ Initial phases were identified using molecular replacement in PHASER.³⁹ The structure was refined using iterative rounds of manual building using COOT⁴⁰ and refinement using PHENIX-REFINE.⁴¹ The refined structure was validated with MolProbity,⁴² and the atomic coordinate files were deposited in the Protein Data Bank with Autodep.⁴³

■ ASSOCIATED CONTENT

📄 Supporting Information

The Supporting Information is available free of charge on the ACS Publications website at DOI: 10.1021/acs.jmedchem.9b00365.

Docking studies, X-ray structure determination of DDR1-**7c**, **7f** KINOMEScan study, antiproliferation study of **7f**, animal body weights in mice with **7f**, synthesis route of **7a** and **7b**, ¹H and ¹³C NMR spectra of compounds **7a–n**, HPLC traces for the representative compounds (PDF)

Molecular formula strings (CSV)

Accession Codes

Atomic coordinates and experimental data for the cocrystal structure of **7c** with DDR1 (PDB ID: 6HP9) will be released upon article publication.

■ AUTHOR INFORMATION

Corresponding Authors

*E-mail: alex.bullock@sgc.ox.ac.uk (A.N.B.).

*E-mail: Rolf.Brekken@UTSouthwestern.edu (R.A.B.).

*E-mail: dingke@jnu.edu.cn (K.D.).

*E-mail: luxy2016@jnu.edu.cn. Phone: +86-20-85223259 (X.L.).

ORCID

Ke Ding: 0000-0001-9016-812X

Xiaoyun Lu: 0000-0001-7931-6873

Author Contributions

¹D.Z., H.H., and D.M.P. contributed equally to this work.

Notes

The authors declare no competing financial interest.

■ ACKNOWLEDGMENTS

The authors appreciate the financial support from National Natural Science Foundation of China (81820108029, 21572230, 81673285, and 81425021), Guangdong Province (2015A030312014, 2015A030306042, and 2016A050502041), Guangzhou city (201805010007), and Jinan University. We also thank Diamond Light Source for beamtime (proposal mx15433), as well as the staff of beamline I04 for assistance with data collection. The SGC is a registered charity (number 1097737) that receives funds from AbbVie, Bayer Pharma AG, Boehringer Ingelheim, Canada Foundation for Innovation, Eshelman Institute for Innovation, Genome Canada, Innovative Medicines Initiative (EU/EFPIA) (ULTRA-DD grant no. 115766), Janssen, Merck KGaA Darmstadt Germany, MSD, Novartis Pharma AG, Ontario Ministry of Economic Development and Innovation, Pfizer, São Paulo Research Foundation-FAPESP, Takeda, and Wellcome (106169/ZZ14/Z).

■ ABBREVIATIONS

DDRs, discoidin domain receptors; ECM, extracellular matrix; EMT, epithelial–mesenchymal transition; RTKs, receptor tyrosine kinases; Trks, tropomyosin receptor kinases; IC₅₀, half-maximal (50%) inhibitory concentration of a substance; DFG, Asp-Phe-Gly; ATP, adenosine triphosphate; K_d, binding constant; HB, hydrogen bond; ABL 1, abelson murine leukemia viral oncogene homolog 1; KIT, C-kit receptor; KRAS, K renin–angiotensin system; Trp53, transformation-related protein 53; PYK2, proline-rich tyrosine kinase 2; PEAK1, pseudopodium-enriched atypical kinase 1; DAPI, 4',6-diamidino-2-phenylindole

■ REFERENCES

- (1) Kleeff, J.; Korc, M.; Apte, M.; La Vecchia, C.; Johnson, C. D.; Biankin, A. V.; Neale, R. E.; Tempero, M.; Tuveson, D. A.; Hruban, R. H.; Neoptolemos, J. P. Pancreatic cancer. *Nat. Rev. Dis. Primers* **2016**, *2*, No. 16022.
- (2) Feig, C.; Gopinathan, A.; Neesse, A.; Chan, D. S.; Cook, N.; Tuveson, D. A. The pancreas cancer microenvironment. *Clin. Cancer Res.* **2012**, *18*, 4266–4276.
- (3) Gouirand, V.; Vasseur, S. Fountain of youth of pancreatic cancer cells: the extracellular matrix. *Cell Death Discovery* **2018**, *4*, No. 1.
- (4) Huang, H.; Du, W.; Brekken, R. A. Extracellular matrix induction of intracellular reactive oxygen species. *Antioxid. Redox Signal.* **2017**, *27*, 774–784.
- (5) Valiathan, R. R.; Marco, M.; Leitinger, B.; Kleer, C. G.; Fridman, R. Discoidin domain receptor tyrosine kinases: new players in cancer progression. *Cancer Metastasis Rev.* **2012**, *31*, 295–321.

- (6) Fu, H. L.; Valiathan, R. R.; Arkwright, R.; Sohail, A.; Mihai, C.; Kumarasiri, M.; Mahasenana, K. V.; Mobashery, S.; Huang, P.; Agarwal, G.; Fridman, R. Discoidin domain receptors: unique receptor tyrosine kinases in collagen-mediated signaling. *J. Biol. Chem.* **2013**, *288*, 7430–7437.
- (7) Leitinger, B. Discoidin domain receptor functions in physiological and pathological conditions. *Int. Rev. Cell Mol. Biol.* **2014**, *310*, 39–87.
- (8) Li, Y.; Lu, X.; Ren, X.; Ding, K. Small molecule discoidin domain receptor kinase inhibitors and potential medical applications. *J. Med. Chem.* **2015**, *58*, 3287–3301.
- (9) Gao, H.; Chakraborty, G.; Zhang, Z.; Akalay, I.; Gadiya, M.; Gao, Y.; Sinha, S.; Hu, J.; Jiang, C.; Akram, M.; Brogi, E.; Leitinger, B.; Giancotti, F. G. Multi-organ site metastatic reactivation mediated by non-canonical discoidin domain receptor 1 signaling. *Cell* **2016**, *166*, 47–62.
- (10) Hur, H.; Ham, I. H.; Lee, D.; Jin, H.; Aguilera, K. Y.; Oh, H. J.; Han, S. U.; Kwon, J. E.; Kim, Y. B.; Ding, K.; Brekken, R. A. Discoidin domain receptor 1 activity drives an aggressive phenotype in gastric carcinoma. *BMC Cancer* **2017**, *17*, No. 87.
- (11) Jin, H.; Ham, I. H.; Oh, H. J.; Bae, C. A.; Lee, D. K.; Kim, Y. B.; Son, S. Y.; Chwae, Y. J.; Han, S. U.; Brekken, R. A.; Hur, H. Inhibition of discoidin domain receptor 1 prevents stroma-induced peritoneal metastasis in gastric carcinoma. *Mol. Cancer Res.* **2018**, *16*, 1590–1600.
- (12) Shintani, Y.; Fukumoto, Y.; Chaika, N.; Svoboda, R.; Wheelock, M. J.; Johnson, K. R. Collagen I-mediated up-regulation of N-cadherin requires cooperative signals from integrins and discoidin domain receptor 1. *J. Cell Biol.* **2008**, *180*, 1277–1289.
- (13) Huang, H.; Svoboda, R. A.; Lazenby, A. J.; Saowapa, J.; Chaika, N.; Ding, K.; Wheelock, M. J.; Johnson, K. R. Up-regulation of N-cadherin by collagen I-activated discoidin domain receptor 1 in pancreatic cancer requires the adaptor molecule shc1. *J. Biol. Chem.* **2016**, *291*, 23208–23223.
- (14) Aguilera, K. Y.; Huang, H.; Du, W.; Hagopian, M. M.; Wang, Z.; Hinz, S.; Hwang, T. H.; Wang, H.; Fleming, J. B.; Castrillon, D. H.; Ren, X.; Ding, K.; Brekken, R. A. Inhibition of discoidin domain receptor 1 reduces collagen-mediated tumorigenicity in pancreatic ductal adenocarcinoma. *Mol. Cancer Ther.* **2017**, *16*, 2473–2485.
- (15) Kothiwale, S.; Borza, C. M.; Lowe, E. W., Jr.; Pozzi, A.; Meiler, J. Discoidin domain receptor 1 (DDR1) kinase as target for structure-based drug discovery. *Drug Discovery Today* **2015**, *20*, 255–261.
- (16) Gao, M.; Duan, L.; Luo, J.; Zhang, L.; Lu, X.; Zhang, Y.; Zhang, Z.; Tu, Z.; Xu, Y.; Ren, X.; Ding, K. Discovery and optimization of 3-(2-(Pyrazolo[1,5-a]pyrimidin-6-yl)ethynyl)benzamides as novel selective and orally bioavailable discoidin domain receptor 1 (DDR1) inhibitors. *J. Med. Chem.* **2013**, *56*, 3281–3295.
- (17) Kim, H. G.; Tan, L.; Weisberg, E. L.; Liu, F.; Canning, P.; Choi, H. G.; Ezell, S. A.; Wu, H.; Zhao, Z.; Wang, J.; Mandinova, A.; Griffin, J. D.; Bullock, A. N.; Liu, Q.; Lee, S. W.; Gray, N. S. Discovery of a potent and selective DDR1 receptor tyrosine kinase inhibitor. *ACS Chem. Biol.* **2013**, *8*, 2145–2150.
- (18) Richters, A.; Nguyen, H. D.; Phan, T.; Simard, J. R.; Grutter, C.; Engel, J.; Rauh, D. Identification of type II and III DDR2 inhibitors. *J. Med. Chem.* **2014**, *57*, 4252–4262.
- (19) Terai, H.; Tan, L.; Beauchamp, E. M.; Hatcher, J. M.; Liu, Q.; Meyerson, M.; Gray, N. S.; Hammerman, P. S. Characterization of DDR2 inhibitors for the treatment of DDR2 mutated non-small cell lung cancer. *ACS Chem. Biol.* **2015**, *10*, 2687–2696.
- (20) Grither, W. R.; Longmore, G. D. Inhibition of tumor-microenvironment interaction and tumor invasion by small-molecule allosteric inhibitor of DDR2 extracellular domain. *Proc. Nat. Acad. Sci. U.S.A.* **2018**, *115*, E7786–E7794.
- (21) Wang, Z.; Bian, H.; Bartual, S. G.; Du, W.; Luo, J.; Zhao, H.; Zhang, S.; Mo, C.; Zhou, Y.; Xu, Y.; Tu, Z.; Ren, X.; Lu, X.; Brekken, R. A.; Yao, L.; Bullock, A. N.; Su, J.; Ding, K. Structure-Based Design of tetrahydroisoquinoline-7-carboxamides as selective discoidin domain receptor 1 (DDR1) inhibitors. *J. Med. Chem.* **2016**, *59*, 5911–5916.
- (22) Ambrogio, C.; Gomez-Lopez, G.; Falcone, M.; Vidal, A.; Nadal, E.; Crosetto, N.; Blasco, R. B.; Fernandez-Marcos, P. J.; Sanchez-Céspedes, M.; Ren, X.; Wang, Z.; Ding, K.; Hidalgo, M.; Serrano, M.; Villanueva, A.; Santamaria, D.; Barbacid, M. Combined inhibition of DDR1 and Notch signaling is a therapeutic strategy for KRAS-driven lung adenocarcinoma. *Nat. Med.* **2016**, *22*, 270–277.
- (23) Wang, Z.; Zhang, Y.; Bartual, S. G.; Luo, J.; Xu, T.; Du, W.; Xun, Q.; Tu, Z.; Brekken, R. A.; Ren, X.; Bullock, A. N.; Liang, G.; Lu, X.; Ding, K. Tetrahydroisoquinoline-7-carboxamide derivatives as new selective discoidin domain receptor 1 (DDR1) inhibitors. *ACS Med. Chem. Lett.* **2017**, *8*, 327–332.
- (24) Skaper, S. D. The Neurotrophin Family of Neurotrophic Factors: An Overview. In *Neurotrophic Factors*; Skaper, S., Ed.; Methods in Molecular Biology (Methods and Protocols); Humana Press, 2012; Vol. 846, pp 1–12.
- (25) Klein, R.; Silos-Santiago, I.; Smeyne, R. J.; Lira, S. A.; Brambilla, R.; Bryant, S.; Zhang, L.; Snider, W. D.; Barbacid, M. Disruption of the neurotrophin-3 receptor gene *trkC* eliminates la muscle afferents and results in abnormal movements. *Nature* **1994**, *368*, 249–251.
- (26) Smeyne, R. J.; Klein, R.; Schnapp, A.; Long, L. K.; Bryant, S.; Lewin, A.; Lira, S. A.; Barbacid, M. Severe sensory and sympathetic neuropathies in mice carrying a disrupted *Trk/NGF* receptor gene. *Nature* **1994**, *368*, 246–249.
- (27) Kahn, M. A.; Kumar, S.; Liebl, D.; Chang, R.; Parada, L. F.; De Vellis, J. Mice lacking NT-3, and its receptor *TrkC*, exhibit profound deficiencies in CNS glial cells. *Glia* **1999**, *26*, 153–165.
- (28) Albaugh, P.; Fan, Y.; Mi, Y.; Sun, F.; Adrian, F.; Li, N.; Jia, Y.; Sarkisova, Y.; Kreusch, A.; Hood, T.; Lu, M.; Liu, G.; Huang, S.; Liu, Z.; Loren, J.; Tuntland, T.; Karanewsky, D. S.; Seidel, H. M.; Molteni, V. Discovery of GNF-5837, a selective TRK inhibitor with efficacy in rodent cancer tumor models. *ACS Med. Chem. Lett.* **2012**, *3*, 140–145.
- (29) Wang, Z.; Zhang, Y.; Pinkas, D. M.; Fox, A. E.; Luo, J.; Huang, H.; Cui, S.; Xiang, Q.; Xu, T.; Xun, Q.; Zhu, D.; Tu, Z.; Ren, X.; Brekken, R. A.; Bullock, A. N.; Liang, G.; Ding, K.; Lu, X. Design, Synthesis, and Biological Evaluation of 3-(Imidazo[1,2-a]pyrazin-3-ylethynyl)-4-isopropyl- N-(3-((4-methylpiperazin-1-yl)methyl)-5-(trifluoromethyl)phenyl)benzamide as a Dual Inhibitor of Discoidin Domain Receptors 1 and 2. *J. Med. Chem.* **2018**, *61*, 7977–7990.
- (30) Fabian, M. A.; Biggs, W. H.; Treiber, D. K.; Atteridge, C. E.; Azimioara, M. D.; Benedetti, M. G.; Carter, T. A.; Ciceri, P.; Edeen, P. T.; Floyd, M.; Ford, J. M.; Galvin, M.; Gerlach, J. L.; Grotzfeld, R. M.; Herrgard, S.; Insko, D. E.; Insko, M. A.; Lai, A. G.; Lelias, J. M.; Mehta, S. A.; Milanov, Z. V.; Velasco, A. M.; Wodicka, L. M.; Patel, H. K.; Zarrinkar, P. P.; Lockhart, D. J. A small molecule-kinase interaction map for clinical kinase inhibitors. *Nat. Biotechnol.* **2005**, *23*, 329–336.
- (31) Huang, H.; Wright, S.; Zhang, J.; Brekken, R. A. Getting a grip on adhesion: Cadherin switching and collagen signaling. *Biochim. Biophys. Acta, Mol. Cell Res.* **2019**, DOI: 10.1016/j.bbamcr.2019.04.002.
- (32) Shintani, Y.; Fukumoto, Y.; Chaika, N.; Grandgenett, P. M.; Hollingsworth, M. A.; Wheelock, M. J.; Johnson, K. R. ADH-1 suppresses N-cadherin-dependent pancreatic cancer progression. *Int. J. Cancer* **2008**, *122*, 71–78.
- (33) Dagogo-Jack, I.; Shaw, A. T. Tumour heterogeneity and resistance to cancer therapies. *Nat. Rev. Clin. Oncol.* **2018**, *15*, 81–94.
- (34) Westcott, J. M.; Prechtel, A. M.; Maine, E. A.; Dang, T. T.; Esparza, M. A.; Sun, H.; Zhou, Y.; Xie, Y.; Pearson, G. W. An epigenetically distinct breast cancer cell subpopulation promotes collective invasion. *J. Clin. Invest.* **2015**, *125*, 1927–1943.
- (35) (a) Rudd, M. L.; Mohamed, H.; Price, J. C.; O'Hara, A. J.; Le, G. M.; Urlick, M. E.; Cruz, P.; Zhang, S.; Hansen, N. F.; Godwin, A. K.; Sgro, D. C.; Wolfsberg, T. G.; Mullikin, J. C.; Merino, M. J.; Bell, D. W. Mutational analysis of the tyrosine kinase in serous and clear cell endometrial cancer uncovers rare somatic mutations in *TNK2* and *DDR1*. *BMC Cancer* **2014**, *14*, No. 884. (b) Davies, H.; Hunter, C.; Smith, R.; Stephens, P.; Greenman, C.; Bignell, G.; Teague, J.; Butler, A.; Edkins, S.; Stevens, C.; Parker, A.; O'Meara, S.; Avis, T.;

Barthorpe, S.; Brackenbury, L.; Buck, G.; Clements, J.; Cole, J.; Dicks, E.; Edwards, K.; Forbes, S.; Gorton, M.; Gray, K.; Halliday, K.; Harrison, R.; Hills, K.; Hinton, J.; Jones, D.; Kosmidou, V.; Laman, R.; Lugg, R.; Menzies, A.; Perry, J.; Petty, R.; Raine, K.; Shepherd, R.; Small, A.; Solomon, H.; Stephens, Y.; Tofts, C.; Varian, J.; Webb, A.; West, S.; Widaa, S.; Yates, A.; Brasseur, F.; Cooper, C. S.; Flanagan, A. M.; Green, A.; Knowles, M.; Leung, S. Y.; Looijenga, L. H.; Malkowicz, B.; Pierotti, M. A.; The, B. T.; Yuen, S. T.; Lakhani, S. R.; Easton, D. F.; Weber, B. L.; Goldstraw, P.; Nicholson, A. G.; Wooster, R.; Stratton, M. R.; Futreal, P. A. Somatic mutations of the protein kinase gene family in human lung cancer. *Cancer Res.* **2005**, *65*, 7591–7595.

(36) Wang, G.; Beigelman, L. FXR Modulators and Methods of Their Use. WO2017147047A1, 2017.

(37) (a) Kabsch, W. XDS. *Acta Crystallogr., Sect. D: Biol. Crystallogr.* **2010**, *66*, 125–132. (b) Leslie, A. G. W.; Powell, H. R. Processing Diffraction Data with MOSFLM. In *Evolving Methods for Macromolecular Crystallography*; Read, R. J., Sussman, J. L., Eds.; NATO Science Series; Springer: Dordrecht, 2007; Vol. 245, pp 41–51.

(38) Evans, P. R.; Murshudov, G. N. How good are my data and what is the resolution? *Acta Crystallogr., Sect. D: Biol. Crystallogr.* **2013**, *69*, 1204–1214.

(39) McCoy, A. J.; Grosse-Kunstleve, R. W.; Adams, P. D.; Winn, M. D.; Storoni, L. C.; Read, R. J. Phaser crystallographic software. *J. Appl. Crystallogr.* **2007**, *40*, 658–674.

(40) Emsley, P.; Lohkamp, B.; Scott, W. G.; Cowtan, K. Features and development of coot. *Acta Crystallogr., Sect. D: Biol. Crystallogr.* **2010**, *66*, 486–501.

(41) Adams, P. D.; Afonine, P. V.; Bunkoczi, G.; Chen, V. B.; Davis, I. W.; Echols, N.; Headd, J. J.; Hung, L. W.; Kapral, G. J.; Grosse-Kunstleve, R. W.; McCoy, A. J.; Moriarty, N. W.; Oeffner, R.; Read, R. J.; Richardson, D. C.; Richardson, J. S.; Terwilliger, T. C.; Zwart, P. H. PHENIX: a comprehensive Python-based system for macromolecular structure solution. *Acta Crystallogr., Sect. D: Biol. Crystallogr.* **2010**, *66*, 213–221.

(42) Chen, V. B.; Arendall, W. B., 3rd; Headd, J. J.; Keedy, D. A.; Immormino, R. M.; Kapral, G. J.; Murray, L. W.; Richardson, J. S.; Richardson, D. C. MolProbity: all-atom structure validation for macromolecular crystallography. *Acta Crystallogr., Sect. D: Biol. Crystallogr.* **2010**, *66*, 12–21.

(43) Yang, H.; Guranovic, V.; Dutta, S.; Feng, Z.; Berman, H. M.; Westbrook, J. D. Automated and accurate deposition of structures solved by X-ray diffraction to the Protein Data Bank. *Acta Crystallogr., Sect. D: Biol. Crystallogr.* **2004**, *60*, 1833–1839.